Seventh Framework Programme
Theme 9 Space FP7-SPA.2009.1.1.02
Monitoring of climate change issues (extending core service activities)

Grant agreement for: Collaborative Project (generic).

Project acronym: **MONARCH-A**

Project title: **MONitoring and Assessing Regional Climate change in High latitudes and the Arctic**

Grant agreement no. 242446
Start date of project: 01.03.10
Duration: 36 months
Project coordinator: Nansen Environmental and Remote Sensing Center, Bergen, Norway

D4.1: Year 2 - Synthesis report of the state and variability of changes in high latitude and Arctic regions including dedicated feedbacks to the GMES core services

Due date of deliverable: 29.02.2012

Actual submission date: 29.02.2012

Organization name of lead contractor for this deliverable: NERSC

Authors: Monarch-A participants

Project co-funded by the European Commission within the Seventh Framework Programme, Theme 6 Environment		
Dissemination Level		
PU	Public	X
PP	Restricted to other programme participants (including the Commission)	
RE	Restricted to a group specified by the consortium (including the Commission)	
CO	Confidential, only for members of the consortium (including the Commission)	

MONARCH-A

**MONitoring and Assessing Regional Climate change in
High latitudes and the Arctic**
Grant agreement n° 242446

Ref: D4.2-y2
Date: 27/03/2012
Issue: 3

ISSUE	DATE	CHANGE RECORDS	AUTHOR
0	08/04/2011	Template	K. Lygre
1	29/02/2012	Final version	"
2	5/3/2012	Clean version	"
3	27/3/2012	Revised	"

MONARCH-A

MONitoring and Assessing Regional Climate change in High latitudes and the Arctic
Grant agreement n° 242446

Ref: D4.2-y2
Date: 27/03/2012
Issue: 3

SUMMARY
A synthesis of the data analysis and modelling work is provided together with the highlights of the main results obtained so far during the first 2 years of the project. A more in-depth and comprehensive synthesis will be undertaken during the final reporting year of the project as more thorough analyses of all data subsets have been performed. The preliminary synthesis is given on a selected subset of Essential Climate Variables (ECVs) arranged according to the 3 main project themes including terrestrial carbon and water fluxes, sea level and ocean circulation and the marine carbon cycle in the high latitude and Arctic regions. In total there are 11 ECVs to be explicitly produced in MONARCH-A, including: - <u>Terrestrial:</u> river discharge, snow cover, ice sheet mass balance and permafrost; - <u>Oceanic:</u> sea ice drift and sea ice volume, sea level, current, ocean color and CO2 partial pressure; - <u>Atmospheric:</u> near surface wind field

MONARCH-A CONSORTIUM

Participant no.	Participant organisation name	Short name	Country
1 (Coordinator)	Nansen Environmental and Remote Sensing Center	NERSC	NO
2	The University of Sheffield	USFD	UK
3	Universität Hamburg	UHAM	NO
4	Centre National de la Recherche Scientifique	CNRS	FR
5	Scientific foundation Nansen International Environmental and Remote Sensing Center	NIERSC	RU
6	Universitetet i Bergen	UiB	NO
7	Danmarks Tekniske Universitet	DTU	DK
8	Institut Francais de Recherche pour l'Exploitation de la Mer	IFREMER	FR

MONARCH-A
MONitoring and Assessing Regional Climate change in High latitudes and the Arctic
Grant agreement n° 242446

Ref: D4.2-y2
Date: 27/03/2012
Issue: 3

Table of Contents

MONARCH-A

MONitoring and Assessing Regional Climate change in High latitudes and the Arctic

Grant agreement n° 242446

Ref: D4.2-y2

Date: 27/03/2012

Issue: 3

List of Figures

MONARCH-A
MONitoring and Assessing Regional Climate change in High latitudes and the Arctic
Grant agreement n° 242446

Ref: D4.2-y2
Date: 27/03/2012
Issue: 3

List of Tables

MONARCH-A
MONitoring and Assessing Regional Climate change in High latitudes and the Arctic
Grant agreement n° 242446

Ref: D4.2-y2
Date: 27/03/2012
Issue: 3

1 Introduction

The synthesis in MONARCH-A is a cross-cutting activity in which an Earth System approach is adopted in order to quantify combined and interrelated changes in terrestrial carbon and water fluxes, sea level and ocean circulation and the marine carbon cycle in the high latitude and Arctic regions. The ultimate goal is to generate a dedicated information package tailored to a subset of multidisciplinary Essential Climate Variables (ECVs) and their mutual forcing and feedback mechanisms associated with changes within both the terrestrial and oceanic domains (Table 1, Appendix). In particular the generation of refined and consistent multidisciplinary time series of:

- river discharge, snow cover, ice sheet mass balance and permafrost;
- sea ice drift and sea ice volume, sea level, current, ocean color and CO2 partial pressure;
- near surface wind field

integrated with tailored information on land cover, fire, sea ice extent and concentration, sea ice thickness, sea surface temperature and sea level will provide tailored information and products to assist climate change research to incorporate the refined and consistent ECVs.

The synthesis includes combining selected time series of ECVs generated in the project together with other existing time series, checked and assessed for consistency. In so doing, variability and trends in these ECVs together with the 3D fields from the reanalyses will be synthesized to establish a more comprehensive quantitative understanding of the climate changes in the high latitude and Arctic region over the last 50-60 years. In particular, this includes:

- New and more accurate characterization of the state and variability of river discharge, snow cover and snow water equivalent, permafrost extent and seasonal variability of frozen ground; sea level and Greenland ice sheet mass loss, ocean currents and sea ice drift as well as ocean mass and heat transport, CO2 partial pressure, and near surface wind field.
- New and better quantification of mutual forcing and feedback mechanisms of the high latitude and Arctic climate system, including natural and anthropogenic contributions;
- New knowledge and support to the attribution of the causes of high latitude and Arctic climate change;
- New knowledge and support to interannual-to-decadal prediction of high latitude climate change, in particular through generation of more accurate initial conditions;
- New knowledge and support to advanced understanding of the two-way connections between global and regional climate change.

The integrated science and technology achievements from the three main research themes together with the results of the synthesis and interaction with the scientific climate change

MONARCH-A
MONitoring and Assessing Regional Climate change in
High latitudes and the Arctic
Grant agreement n° 242446

Ref: D4.2-y2
Date: 27/03/2012
Issue: 3

community will make a new advanced knowledge base that can feed into an overall assessment of priorities, design and implementation of a high latitude and Arctic monitoring system for climate change. This will be reported in the forthcoming synthesis reports and is essential for future advances in operational decadal scale prediction and services targeted the high latitude and Arctic regions.

The scope of the present report is to provide a status of the data analysis and modelling work and the highlights of the main results obtained so far in the project.

MONARCH-A
MONitoring and Assessing Regional Climate change in High latitudes and the Arctic
Grant agreement n° 242446

Ref: D4.2-y2
Date: 27/03/2012
Issue: 3

2 Changes in terrestrial carbon and water fluxes

High latitude regions are predicted to suffer much greater warming than lower latitudes as a result of climate change, leading to drastic changes in the carbon and water balance of the region, with associated large effects on snow cover, soil freeze-thaw periods, soil moisture, permafrost, growing season, vegetation cover (including species changes), greenhouse gas fluxes and albedo. Of crucial concern are the feedbacks between these land surface processes and climate warming; this is recognised as one of the greatest sources of uncertainty in climate prediction (IPCC 2007).

2.1 Vegetation cover

Land cover is a crucial determinant of land-atmosphere fluxes, while changes in fire regimes are both an indicator of climate change and are likely to be strongly affected by climate change, with consequences for carbon emissions and sequestration.

A key aim is to amalgamate the separate observations of these different variables in a single modelling framework to elucidate their interactions, involving new modules to ensure that these data can be exploited in hydrological models, Dynamic Vegetation Models and climate models that are fully coupled to a dynamic land surface model.

The Plant Functional Type (PFT) distribution in most Dynamic Vegetation Models (DVM) is obtained by input vegetation cover maps acquired from Earth Observation data. The most important vegetation cover data sets have been inter-compared and used to drive a DVM to establish carbon fluxes sensitivity to input land cover and pinpoint uncertainties caused by translating land classes of the different classifications to model PFTs. The DVM used was the Sheffield Dynamic Global Vegetation Model (SDGVM) (Woodward & Lomas, 1994) and the 5 land cover data sets examined were GlobCover, MODIS LC-VCF, MODIS LC, GLC2000 and one produced for the purposes of the ESA DUE Permafrost project. For comparison the PFT distribution from the LPJ-WM (Wania et al., 2009) are also presented which, unlike most models, doesn't rely on input vegetation cover but simulates its own PFT distribution.

Significant differences were observed (**Figure 1**), with MODIS LC-VCF having the highest coverage of grass and the lowest in both tree and bare ground. The best agreement was between GlobCover and MODIS LC, with GLC2000 having the highest tree cover. Despite GLC2000 and LPJ-WM having similar cumulative cover their vegetation maps show that the spatial distribution is quite different due to the establishment and competition processes of LPJ-WM.

	MONARCH-A	Ref: D4.2-y2
![Monarch-A logo]	MONitoring and Assessing Regional Climate change in High latitudes and the Arctic	Date: 27/03/2012
	Grant agreement n° 242446	Issue: 3
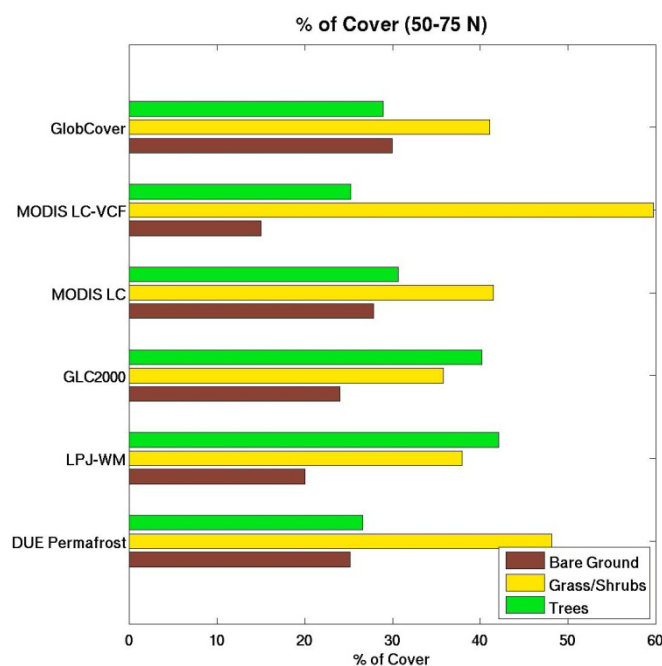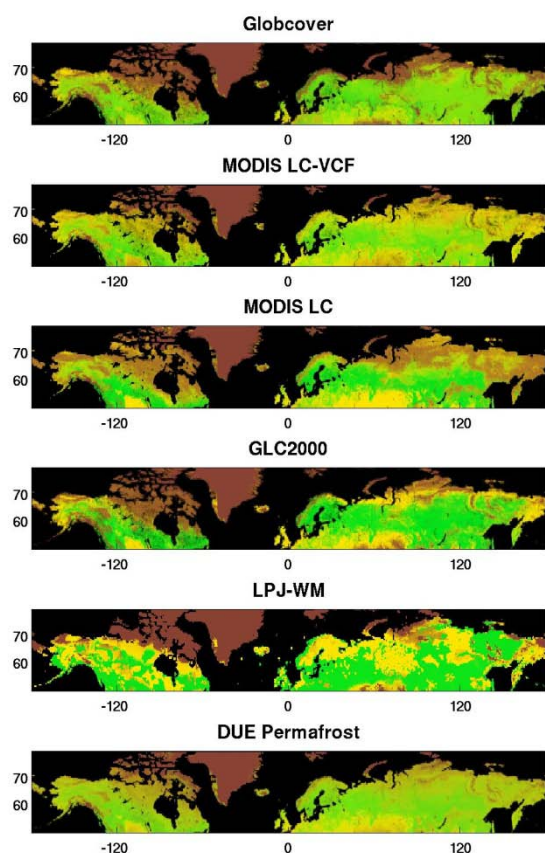
Figure 1. (left) Vegetation maps of the boreal latitudes produced by the 5 land cover data sets that were used to drive SDGVM. Also shown is the natural vegetation produced by LPJ-WM. (**right**) Fraction of tree, grass and bare ground cover for the 5 land cover data sets and natural vegetation of LPJ-WM.

Results of the 5 SDGVM runs driven with the different land covers are presented in **Figure 2** for boreal latitudes. As expected, Net Primary Production (NPP) and consequently heterotrophic respiration (Rh) are found to negatively correlate with the percentage of bare ground cover. MODIS VCF shows the greatest productivity of the 5 land covers with 9.39 Pg C y^{-1}, approximately 10% more than GlobCover, which had the lowest. Since SDGVM treats as fuel only the above-ground biomass, fire emissions are predominantly a linear function of tree cover. The biggest difference can be found between GLC2000 (40% tree cover) and MODIS VCF (25% tree cover) with the latter emitting almost 50% less carbon due to its lower tree coverage. Net Biome Production (NBP) was found to be a linear function of tree and grass cover given by NBP=5.73*(Tree Cover) +2.09*(Grass Cover) +0.71 and R^2=0.86 with NBP in x10^{14} g C, which lead to substantial differences of up to 20% between the lowest carbon uptake by GlobCover and highest by GLC2000. This work highlights the importance of input land cover into a DVM by establishing and quantifying to a certain extent the sensitivity of simulated carbon pools to input vegetation cover.

MONARCH-A
**MONitoring and Assessing Regional Climate change in
High latitudes and the Arctic**
Grant agreement n° 242446

Ref: D4.2-y2
Date: 27/03/2012
Issue: 3
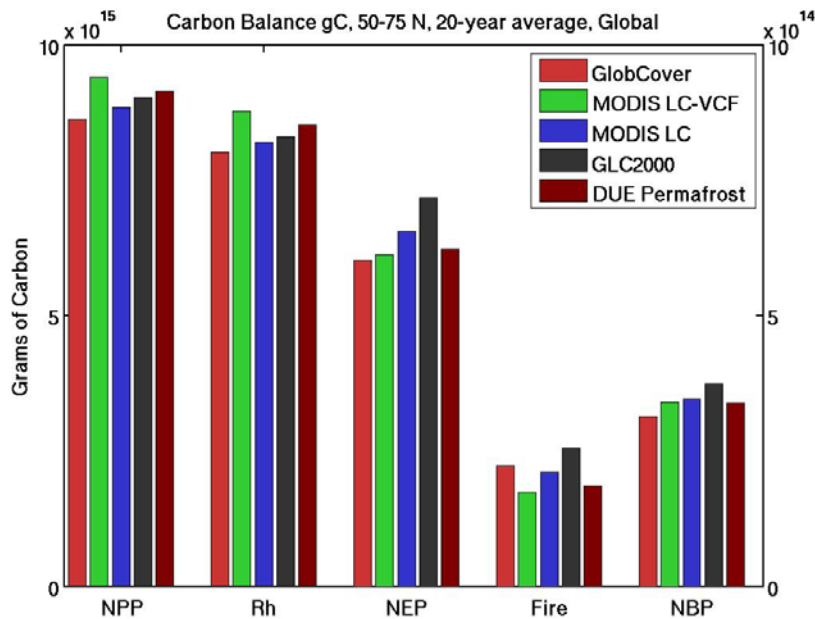
Figure 2. NPP, Rh, NEP, Fire Emissions and NBP outputs of SDGVM when driven with GlobCover, MODIS LC-VCF, MODIS LC,GLC2000 and DUE Permafrost.

2.2   Fire

Data-model comparisons of burned area and fire emissions (**Figure 3**) revealed that although some models capture the magnitude, none of them manages to capture the inter-annual variability (IAV) of the fire emissions or burned area due to the models' deterministic approach towards the stochastic phenomenon of naturally occurring fires.

MONARCH-A
**MONitoring and Assessing Regional Climate change in
High latitudes and the Arctic**
Grant agreement n° 242446

Ref: D4.2-y2
Date: 27/03/2012
Issue: 3
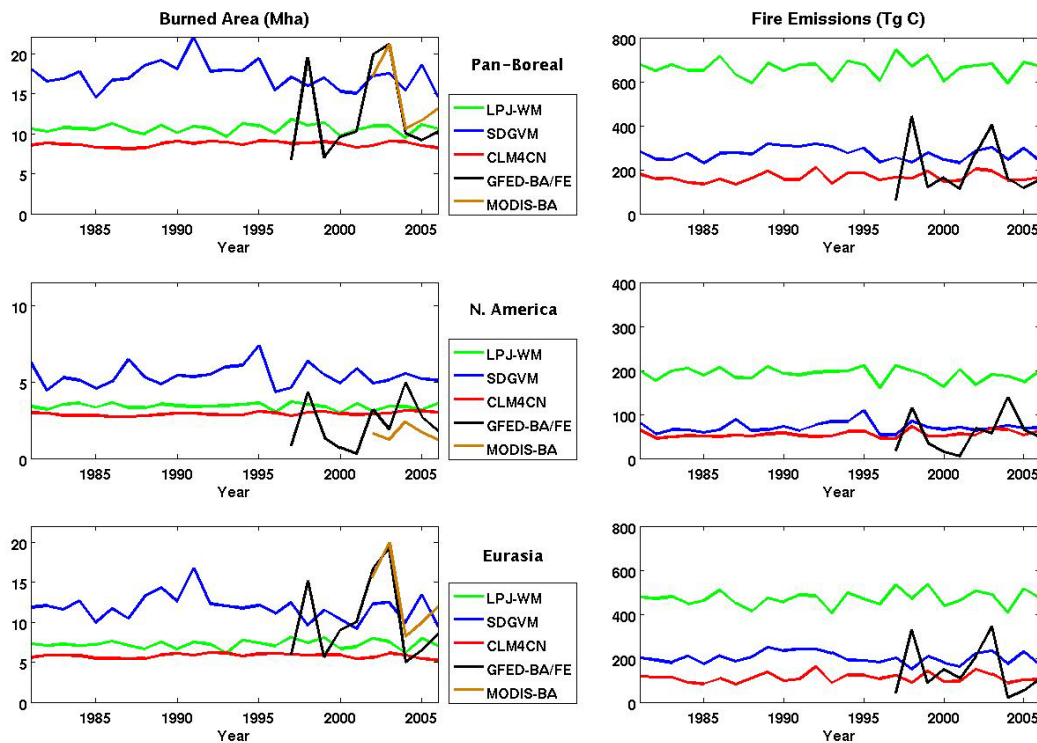
Figure 3. (left) Total area burnt per year (Mha yr^{-1}) for the pan-boreal region, N. America and Eurasia as calculated by the models LPJ-WM, SDGVM and CLM4CN and given by the EO data sets GFED (Global fire emissions database) and MODIS MCD45A1 **(right)** The corresponding fire emissions in (TgC yr^{-1}) for the 3 models and GFED. For both variables the EO data sets exhibit considerably higher variability.
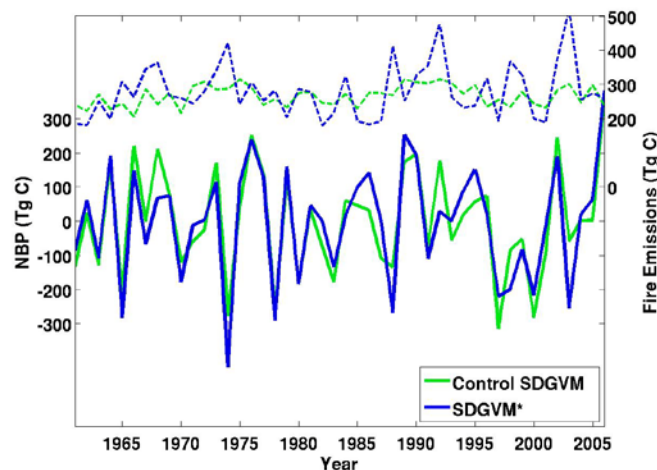
Figure 4. Time series (1960-1996) of the de-trended NBP (solid line, left y-axis) and fire emissions (dashed line, right y-axis) for a control and adjusted SDGVM run parameterized to include the IAV of GFED-BA.

To investigate possible effects on the IAV of the Net Biome Production (NBP) the fire regime of SDGVM was altered in order to include the IAV of the burned area obtained from EO data.

MONARCH-A

MONitoring and Assessing Regional Climate change in High latitudes and the Arctic
Grant agreement n° 242446

Ref: D4.2-y2
Date: 27/03/2012
Issue: 3

As **Figure 4** suggests, although there is a distinctive increase in the IAV of the fire emissions when the EO data variability is injected into the model (SDGVM), the magnitude of the IAV of the NBP is not significantly affected. Although the IAV of burnt area now corresponds more closely to that of the observations, the mean behaviour and trends of NBP remain unaffected. This supports the theorized premise in climate studies that the variability of NBP is not caused, at least to a great degree, by the temporal and spatial variability of fire emissions.

2.1 River discharge and water bodies

The decadal dynamics of high latitude rivers and water bodies have strong global impact, as the huge numbers of lakes forming in the summer season at high latitudes are important for greenhouse gas exchange, evapo-transpiration, runoff and groundwater, and runoff is a major source of fresh water to the Arctic Ocean. In addition, snow cover, snow depth and snow cover period are all indicators of climate change, but also have strong effects on water availability for plant growth, vegetation growing periods, flow of fresh water into the Arctic Ocean and albedo.

To provide long time-series of measurements of water levels over large Arctic rivers and lakes we have assembled the data sets from the different satellite radar altimeters (Topex/Poseidon, ERS, ENVISAT, Jason1/2) and we have computed surface water levels variability for large Arctic rivers and lakes. Processed time series of the lake and river level have been obtained from the Hydroweb web site [http://www.legos.obs-mip.fr/en/equipes/gohs/resultats/i_hydroweb].

River discharge is estimated by combining altimetric observations of water level and historical in situ data on river discharge, see e.g. Kouraev et al., 2004. The Ob' - one of the largest Eurasian rivers – was chosen in order to estimate the accuracy of the T/P altimetric measurements of river level and discharge. Relationships between satellite-derived water level and river discharge measurements at Salekhard gauging station near the Ob' estuary have been established. The introduction of new retracking algorithms for computing the river level will significantly increase the accuracy of the discharge estimates.

Ob' river (ENVISAT radar altimetry) Ice2 retracker data have been used to identify 58 virtual stations along the main channel of the Middle and Lower Ob'. Average values from 2002 to 2009 for each station show the along-river variability of amplitude and maximal and minimal water level (**Figure 6**). We observe a general decrease of both absolute values of water level (eroding effect of the river) and amplitude (widening of the river channel) toward the outlet. Irregularities and spikes may be related to river valley width, influence of confluents etc.

MONARCH-A
**MONitoring and Assessing Regional Climate change in
High latitudes and the Arctic**
Grant agreement n° 242446

Ref: D4.2-y2
Date: 27/03/2012
Issue: 3
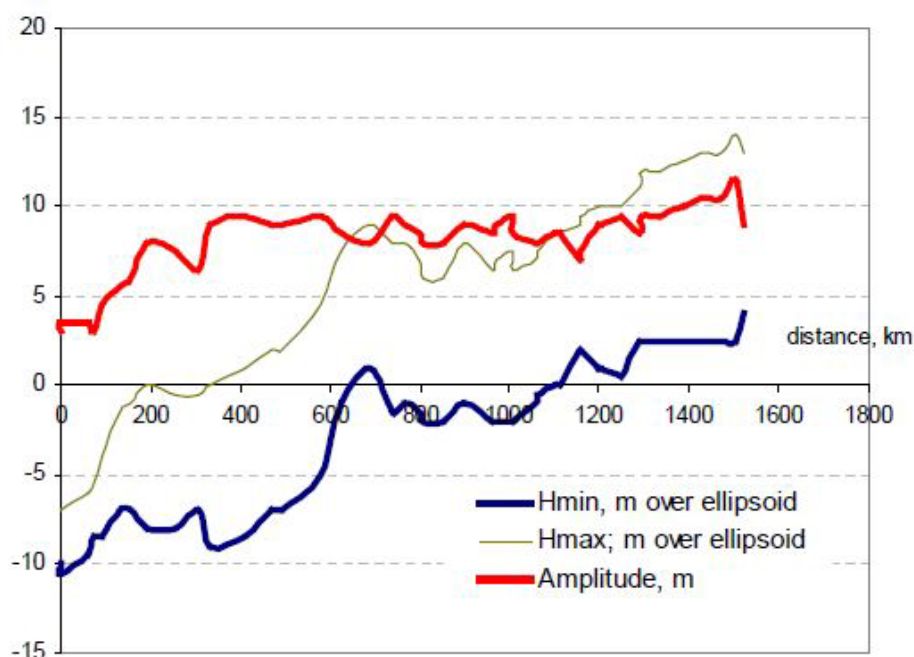
Figure 5. Water level variability along the Lower and Middle Ob' (maximal and minimal values, as well as amplitude). Averaged data for 2002-2009. Distance is expressed in km starting from the northernmost virtual station

An important ingredient in the determination of timing of runoff is the defining of the timing of specific ice events over lakes and seas. By a 3-step method described in Monarch-A Delivery report 2.1.4 the whole altimetric and SSM/I satellite dataset has been processed. The combined altimetric-SSM/I observations significantly enhance the potential of microwave measurement for ice studies. The resulting classification maps for each pentad enables one to define specific dates of ice events (the first appearance of ice "First Ice", the formation of stable ice cover "Ice 100%", the first appearance of open water "First Open Water" and the complete disappearance of ice "Open Water 100%") for each water body or its sub-region, as shown by an example in **Figure 6**, for Lake Baikal (three sub-regions – Northern (NB), Middle (MB) and Southern (SB)), Onega and Ladoga lakes, Aral sea (Northern and Southern parts) and Caspian sea (Western and Eastern parts).

MONARCH-A
MONitoring and Assessing Regional Climate change in High latitudes and the Arctic
Grant agreement n° 242446

Ref: D4.2-y2
Date: 27/03/2012
Issue: 3
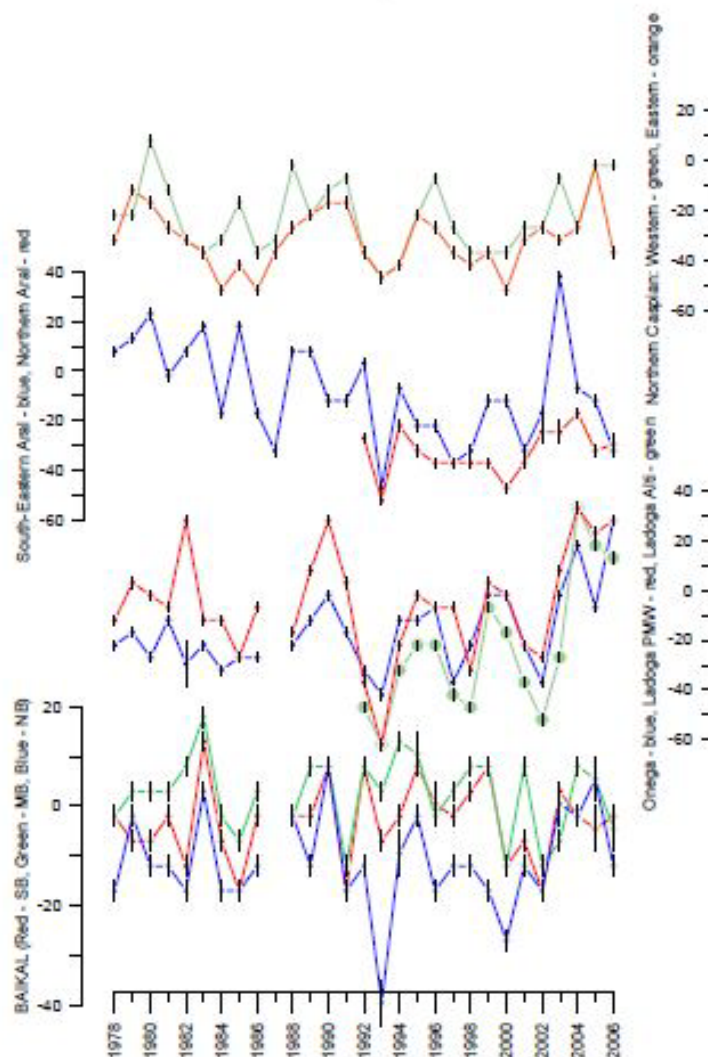
Figure 6. Beginning of ice events (first ice observed), days since 31 December for the five selected water bodies. Dates are expressed as days since 31 December (1=1st of January). In some cases dates are blanked (data availability and/or quality issues). For the Northern Caspian sea, where ice drift is observed throughout the whole winter, dates for Full Ice and First open water have not been defined.

2.4 Snow cover

23 years of SSM/I satellite data set from 1988 to 2010 have been assembled and analysed, computing snow extent, start and end dates of snow cover snow depth and snow water equivalent (**Figure 7**). Data for 5-day and monthly snow extent fields and yearly start and end dates of snow cover for the boreal regions north of 36° latitude are available. Here it is focused on:

- 5-day and monthly snow depth fields for the boreal regions north of 50° latitude.
- 5-day and monthly snow water equivalent fields for the boreal regions north of 50° latitude.

MONARCH-A
MONitoring and Assessing Regional Climate change in High latitudes and the Arctic
Grant agreement n° 242446

Ref: D4.2-y2
Date: 27/03/2012
Issue: 3

Snow Depth (mm)   Snow density (kg/m3)   Snow Water Equivalent (kg/m²)
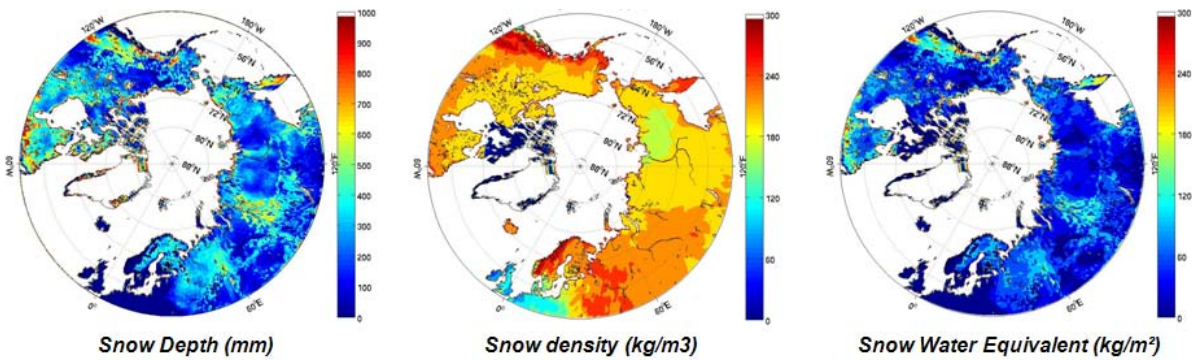
Figure 7. Snow depth (left) Snow density (middle) and snow water equivalent (right) for pentad from 20th to 25th February 2008.

Snow water equivalent is a quantity easier to compare to models. For 2006 comparisons have been made with both the LPJ and SDGVM models (**Figure 8**; Lund-Potsdam-Jena (LPJ), Sheffield Dynamic Global Vegetation Model (SDGVM)). Satellite observations see less snow than both models but present similar seasonal behavior. Fractions of Water are also computed with satellite passive sensors during July and August over the 23 years. This variable is complementary to snow to better understand the water cycle and its dynamics in boreal regions. The annual trends in snow cover are for both models seen to be weakly negative over the observation period, however not significant, as the interannual variability is notable **Figure 9**.
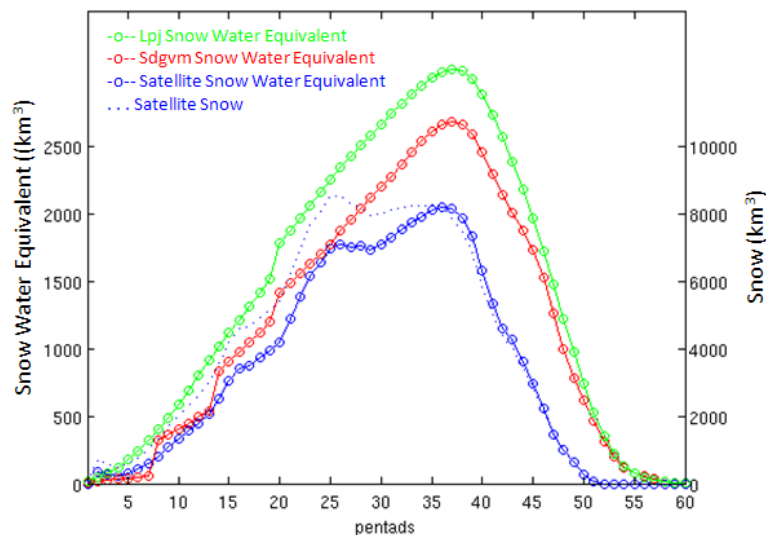
Figure 8 Snow Water Equivalent for Satellite observation (blue), LPJ model (green) and SDGVM (red) and snow volume for satellite observation for year 2006 and over 50°N

MONARCH-A
MONitoring and Assessing Regional Climate change in High latitudes and the Arctic
Grant agreement n° 242446

Ref: D4.2-y2
Date: 27/03/2012
Issue: 3
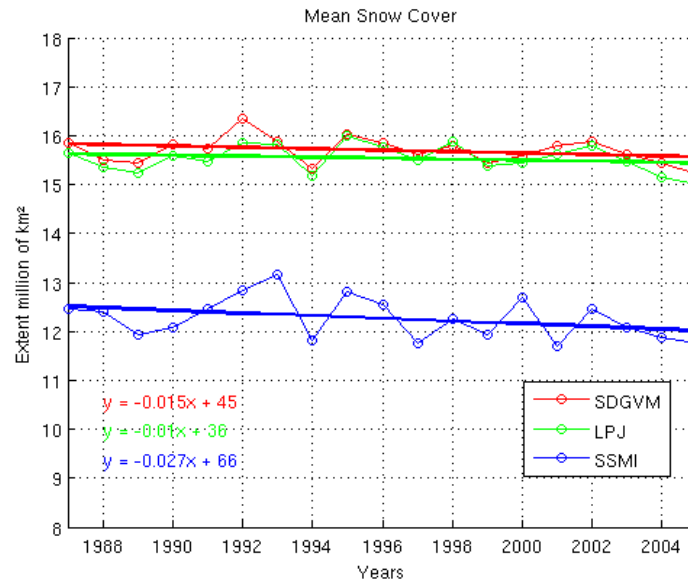
Figure 9. Time series and trends of the annual mean snow cover measured (blue), simulated by LPJ (green) and by SDGVM (red)

2.2 Permafrost

Boreal latitudes are characterized by huge expanses of boreal forest, wetlands, peatlands and tundra lying on organic soils that account for 50% of the global below-ground organic carbon. All these various biomes are to some extent underlain by permafrost (continuous, widespread or scattered) which makes it important for land models to incorporate processes that simulate permafrost formation and dynamics, including its effect on hydrology. The LPJ-WM model outputs of permafrost parameters have been compared with data collected from various sources which were amalgamated into reference maps.

The reference map has been developed based on scanned and digitized permafrost maps published from 1970 to 1988, yielding permafrost boundary, permafrost depth, temperature of permafrost and active layer thickness. Practically the reference map is a collection of five different maps (for Russia, Mongolia, China, Canada and Alaska) that are difficult to merge because of differences in permafrost thickness and temperature classification.

For the Russian territory the digital map describes permafrost boundary, permafrost depth (contours for 25 m, 50 m, 100 m, 200 m, 300 m, 500 m, 700 m and 900 m), the temperature of permafrost, and the active layer thickness (**Figure 10**), based on the I. Baranov's paper map published in 1970 at a scale of 1:5,000,000, still not well known in the international scientific community. Local - although not consistent - data describing different permafrost parameters have also been collected.
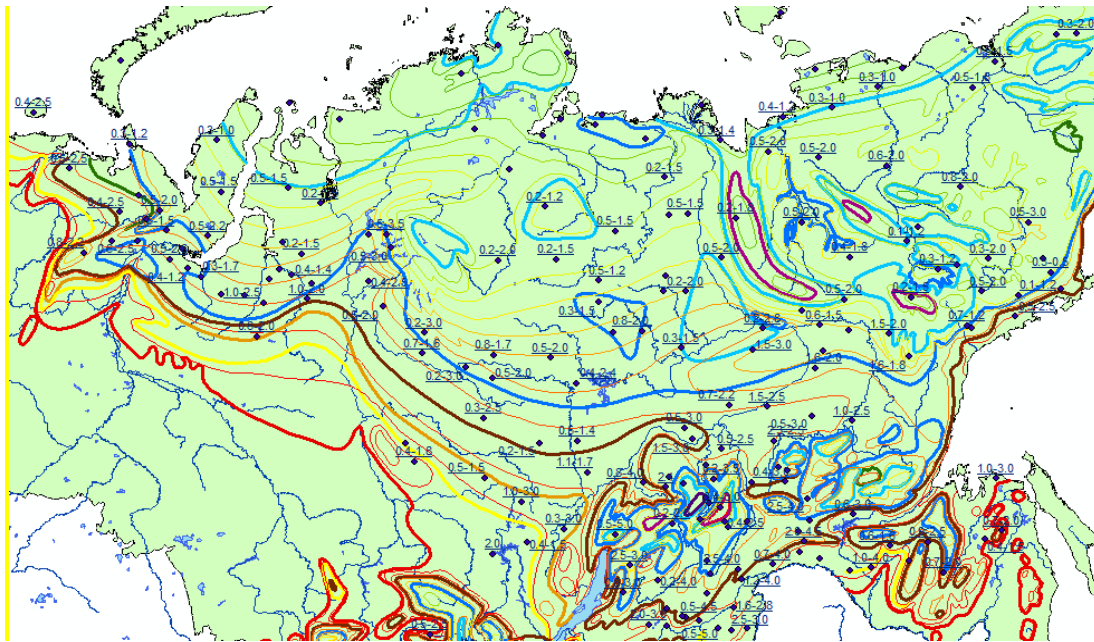
Figure 10. Digital permafrost map of Russia. Digitized parameters: permafrost boundary, depth, temperature and active layer.

Collection and analyzing of data that describe permafrost parameter changes has been initiated for the period from 80th of the previous century to present. Data on active layer and ground temperature on different levels for the Russian territory has been collected and processed. The data is transformed into the common XLS format. All time series are illustrated by charts.

Figure 11 depicts how LPJ-WM correctly captures the permafrost extent both for N. America and Eurasia.
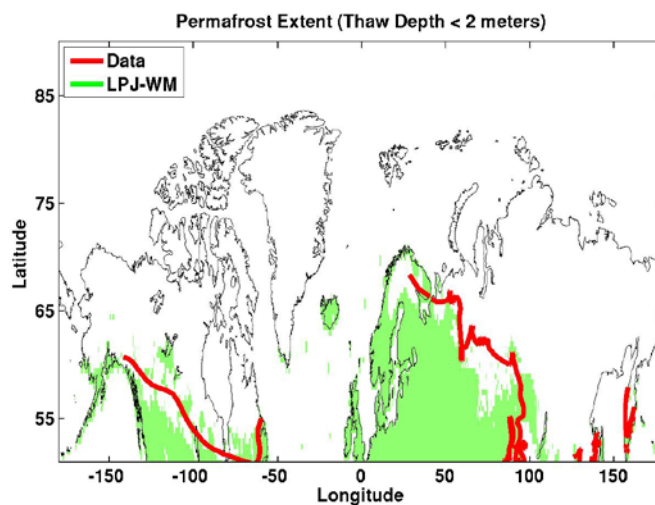
Figure 11. Comparison of permafrost extent over the boreal latitudes obtained from LPJ-WM and reference maps.

MONARCH-A

MONitoring and Assessing Regional Climate change in High latitudes and the Arctic
Grant agreement n° 242446

Ref: D4.2-y2
Date: 27/03/2012
Issue: 3

Figure 12 shows that the model adequately simulates permafrost temperature for Eurasia, albeit with an offset which increases as permafrost temperature decreases. Permafrost depth cross-correlation between data and model could not be carried out as LPJ-WM doesn't simulate this parameter, while lack of metadata on active layer depth maps didn't permit a data-model comparison for this parameter either. Although the model successfully captures permafrost extent and to some degree permafrost temperature, it was found that fire parametrization prohibits the model from correctly simulating the response of permafrost to fire disturbance.
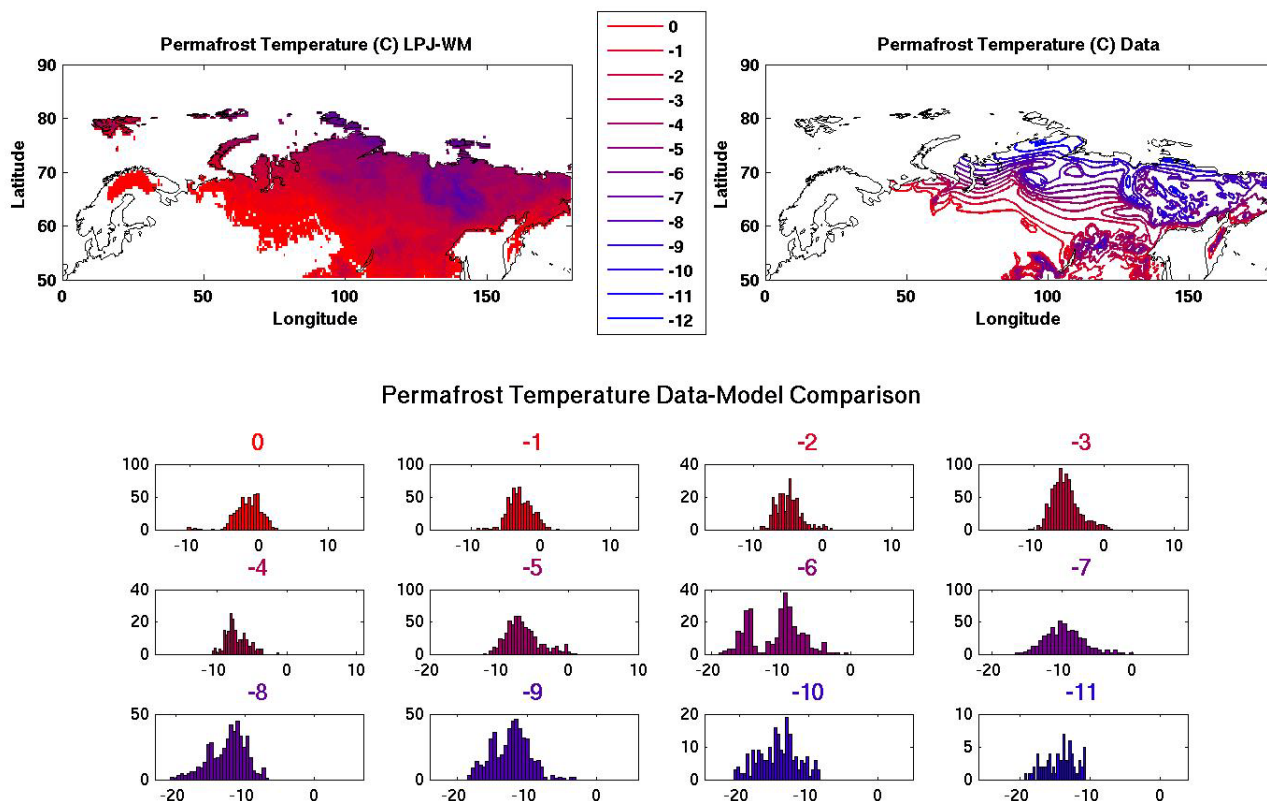
Figure 12. Comparison of permafrost temperature over Eurasia obtained from LPJ-WM and historical maps. Histograms were obtained by plotting the model values underlying the contours of the data for each temperature class.

MONARCH-A

MONitoring and Assessing Regional Climate change in High latitudes and the Arctic
Grant agreement n° 242446

Ref: D4.2-y2
Date: 27/03/2012
Issue: 3

3   Changes in sea level and ocean circulation

3.1   Ice sheets and glaciers

Current mass loss from the Greenland ice sheet is estimated to be around 205 +/- 20 GT/year, corresponding to about 0.8 mm/year sea level rise, with a possible acceleration in the northwest of Greenland. In comparison the loss in Antarctica is about 100 +/- 50 GT/year.

A key question is whether the corresponding freshwater flux will change the sub-polar gyre and whether this impacts the northward flowing Atlantic Water.

Spatial–temporal variability and changes of Greenland ice sheet elevation from 1992 to 2008 are analyzed from consistently merged ERS-1, ERS-2 and Envisat satellite radar altimeter data. The elevation time series has been adjusted for its dependence on backscatter coefficient (σ^0) based on the approach by Davis and Ferguson, 2004 and Zwally et al., 2005 in order to account for the changes in the ice sheet surface properties. By this the amplitude of elevation seasonal variations is reduced substantially and the local elevation change-rate estimates are corrected by up to several cm/year.

The sensitivity of measured elevation to changes in σ^0 was estimated by using the differences between adjacent points of time series as in (Khvorostovsky, 2011). Temporal variations of this sensitivity and adjustment of elevation time series for dependence on other waveform shape parameters are not taken into account here.

Temporal variations show that increases in surface elevation from 1995 observed over the high-elevation regions of Greenland were followed by an elevation decrease from 2006 (Johannessen et al., 2005; Khvorostovsky, 2011). In contrast, over low-elevation areas below 1500 m the surface elevation decrease that started from 2000 has continued (**Figure 13**). Dataset presented here gives an average elevation change rate of 3.2 ± 0.2 cm/year from 1992 to 2008 over 76% of the Greenland ice sheet area. However marginal areas are not completely measured by radar altimetry and substantial thinning rates over these areas could offset the observed average elevation change. At the same time spatio-temporal analysis reveals large interannual elevation variability over western and south-eastern regions.
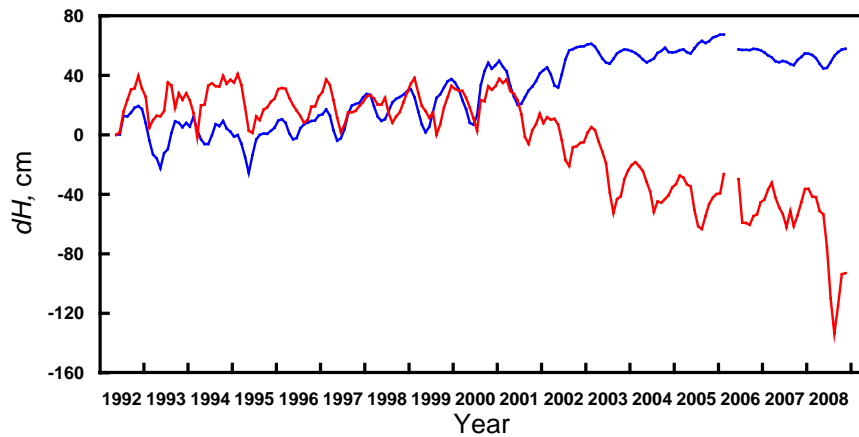
Figure 13. Elevation time series over the areas above (blue) and below (red) 1500 m obtained by merging ERS-1, ERS-2 and Envisat satellite altimeter measurements from 1992 to 2008.
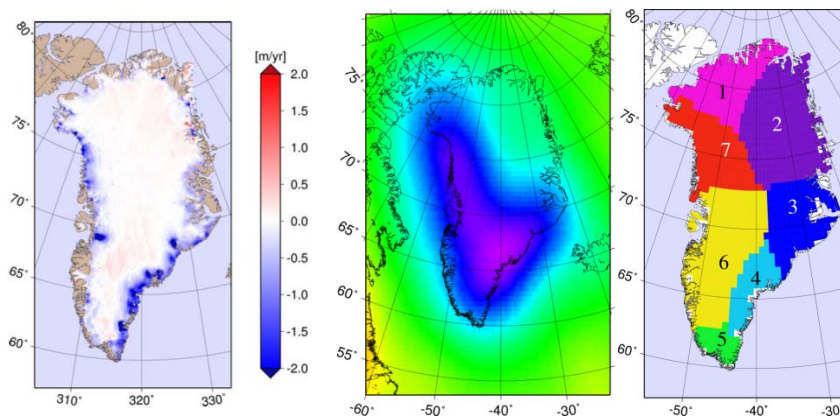
Figure 14. Observed mean elevation changes from ICESat (left) and gavity changes observed by GRACE (middle) over the period 2003-2008. Definition of seven major drainage basins (right)
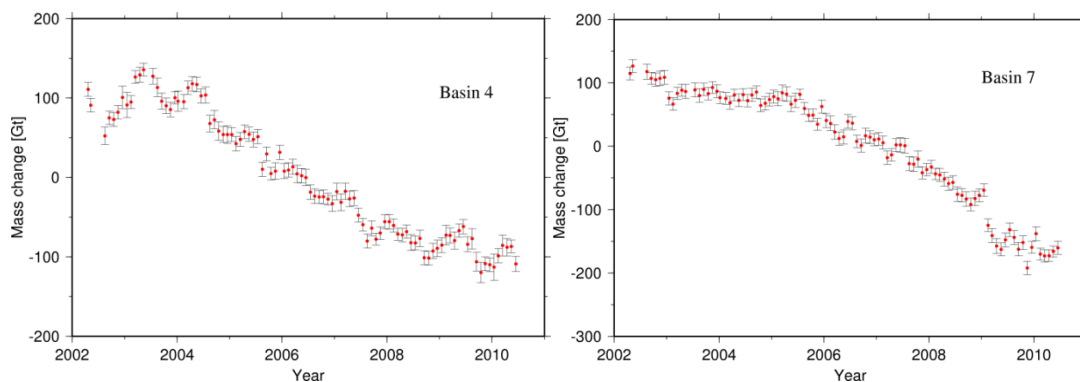
Figure 15. Time series of GRACE based mass changes for basin 4 and 7

MONARCH-A
MONitoring and Assessing Regional Climate change in High latitudes and the Arctic
Grant agreement n° 242446

Ref: D4.2-y2
Date: 27/03/2012
Issue: 3

Surface heights have also been derived from NASA's laser altimetry satellite mission ICESat (L. S. Sørensen, 2011) for October 2003 – March 2008, **Figure 14** left. A distinct thinning of the ice sheet is found along the southeast and west coasts, and a smaller but consistent thickening is found in the interior part of the ice sheet, in agreement with the trends derived from ERS/ENVISAT.

The joint American-German GRACE gravity satellite mission has measured the Earth gravity field, since 2002. A generalized inversion method has been used to estimate the Greenland Ice Sheet mass changes Fig. 2 middle (Forsberg, Barletta and Sørensen, 2011). The estimate for the entire ICESat period (October 2003-March 2008) is -204 +/- 21 Gt/yr. Conversion of the ICESat heights into mass changes using firn densification and snow density models, results in a larger estimate of -240 +/- 28 Gt/yr. Work to estimate the freshwater contribution to the Arctic Ocean from GRACE data is ongoing (Barletta and Sørensen). The contribution from the Greenland Ice Sheet will be estimated for each of the seven major basins presented in **Figure 14** right, adapted from Hardy et al, 2000. Examples of mass changes for basin 4 and 7 are given in **Figure 15**, both showing a negative trend/mass balance.

First results of near-coincident CryoSat-2 (level 2) and airborne laser scanner data over the Greenland Ice Sheet (Sørensen et al, 2011) is not consistent and show biases between the two data sets by up to 50m. This is believed to improve with the reprocessed data using the updated ground processor, which are about to be implemented at the time of writing.

3.2   Sea level

A main goal with the sea level observations and modelling is together with other parameters to provide dynamically consistent reanalysis of the Arctic Ocean over the last 50 years, allowing better understanding of water mass formation, circulation, sea level, sea ice extent and sea ice thickness changes in this region.

During the past few decades, the Arctic region has warmed at a faster rate than the rest of the globe in response to anthropogenic climate change (IPCC, 2007). Increase air temperature (e.g., Chylek et al., 2010), sea ice extent and thickness decrease (e.g., Kwok et al., 2009, Stroeve et al., 2010) and Greenland ice sheet mass loss (e.g., Holland et al., 2008, Rignot et al., 2011) are among the most visible effects of global warming in the Arctic. As sea level is a very sensible indicator of climate change and variability, one may also wonder whether Arctic sea level is rising at a rate different than the global mean sea level and what are the main patterns of regional variability. Only a few studies have been dedicated to study Arctic sea level (Proshutinsky et al. 2001, 2004). Proshutinsky et al. (2004) estimated sea level change in the Russian sector of the Arctic Ocean using tide gauge data released in 2003 by the Arctic and Antarctic Research Institute in St Petersburg (Russia). These authors

MONARCH-A
MONitoring and Assessing Regional Climate change in High latitudes and the Arctic
Grant agreement n° 242446

Ref: D4.2-y2
Date: 27/03/2012
Issue: 3

found that over ~1950-2000, the mean sea level along the Russian coastlines rose at a mean rate of 1.85 mm/yr after correcting for the Glacial Isostatic Adjustment (GIA) process.

Sea level change and variability have been investigated in part of the Arctic region over the 1950 2009 period. Coastal mean sea level (corrected for GIA and inverse barometer effects) in the Norwegian and Russian areas was almost stable until about 1980 but since then displayed a clear increasing trend (**Figure 16**).
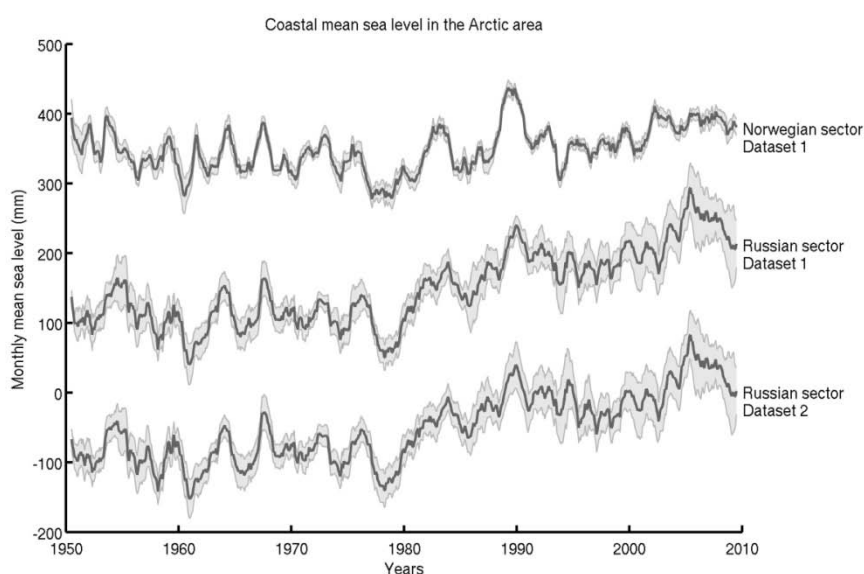
Figure 16. MSL curves in the Norwegian (dataset1) and Russian sectors (dataset1 and 2)

Until the mid-1990s, the mean coastal sea level closely follows closely the fluctuations of Arctic Oscillation (AO) index, but not thereafter. Since 1995, the coastal mean sea level (average of the Norwegian and Russian tide gauge data) presents an increasing trend of ~4 mm/yr. Using in situ ocean temperature and salinity data down to 700 m from three different data bases, we estimated the thermosteric, halosteric and steric (sum of thermosteric and halosteric) sea level since 1970 in the North Atlantic and Nordic Seas region, as well as along the Norwegian coast (incomplete data coverage prevented us to analyze steric data along the Russian coast)

We note a strong anti-correlation between the thermosteric and halosteric components (**Figure 17**) both in terms of spatial trends and regionally averaged time series. The latter show a strong change as of ~1995 that indicates simultaneous increase in temperature and salinity, a result confirmed but the Empirical Orthogonal Function decomposition over the studied region. Regionally distributed steric data are compared to altimetry-based sea level over 1993-2009, whose spatial trend patterns can be largely explained by steric patterns,

MONARCH-A
**MONitoring and Assessing Regional Climate change in
High latitudes and the Arctic**
Grant agreement n° 242446

Ref: D4.2-y2
Date: 27/03/2012
Issue: 3

even if residual spatial trends suggest that other factors as regional ocean mass changes contribute.
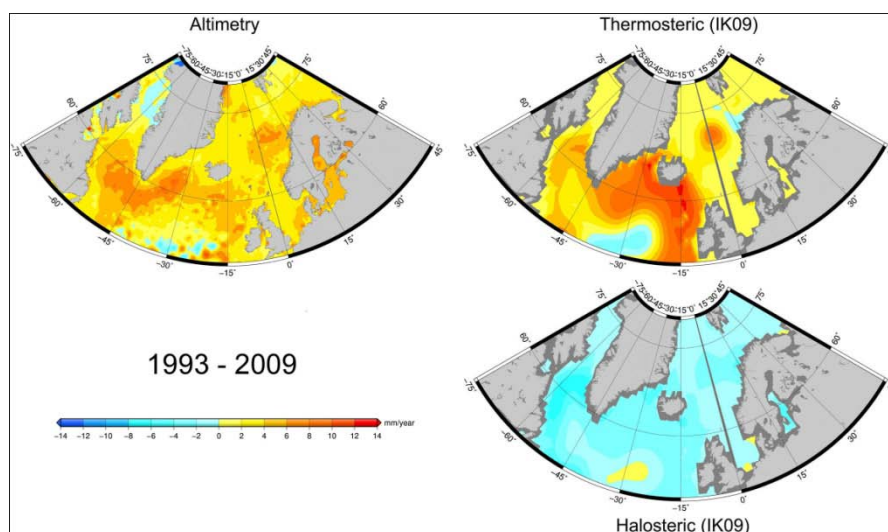
Figure 17. Altimetry-based, thermosteric and halosteric sea level trend patterns in the North Atlantic and Nordic Seas region over 1993-2009.

Comparing the observed coastal mean sea level with the steric sea level and the ocean mass component estimated with GRACE space gravimetry data (since 2003), it can be concluded that the mass component plays a significant role and partly explains the sustained sea level rise (of ~4 mm/yr) observed over the altimetry era in that particular area (**Figure 18**).
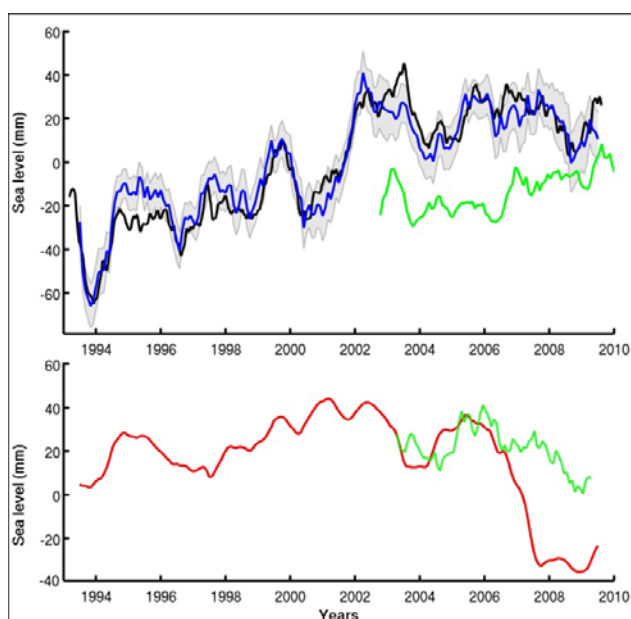
Figure 18. Top: Tide gauge-based (blue curve) and altimetry-based CMSL (black curve) at the Norwegian tide gauge sites sector over 1993-2009. The green curve represents the GRACE-based

MONARCH-A
MONitoring and Assessing Regional Climate change in High latitudes and the Arctic
Grant agreement n° 242446

Ref: D4.2-y2
Date: 27/03/2012
Issue: 3

mean ocean mass component. Bottom: mean steric sea level (IK09 data); the green curve represents the steric component estimated from the difference between tide gauge-based CMSL and GRACE mean ocean mass

Modelled SSH. Model values of sea surface height (SSH) have been compared for 1970-2007 with estimates of Kwok et al., (2011), obtained on the basis of six years (2004-2008) ICESat satellite observations. Generally models reproduce overall spatial structure of the SSH in the Arctic ocean with higher values in Amerasian part of the basin and lower values in Eurasian part (**Figure 19**). Differences in SSH values between these two basins are about 80-100 cm, in agreement with Kwok et al., (2011).

3.3 Current

As a first step towards Arctic Ocean reanalysis several existent long-term model simulations are exploited and evaluated. The participating models include:

- Regional setup of MITgcm model ATL (Serra et al., 2010) in three different resolutions from the Institute of Oceanography, University of Hamburg
- Regional setup of MICOM model (Hátún et al., 2005) from the Nansen Environmental and Remote Sensing Center.
- Global setup of MPIOM model (project STORM https://verc.enes.org/community/projects/national-projects/german-projects/storm/) from the Max Planck Institute for Meteorology.

![MonarcH-A logo]

MONARCH-A
**MONitoring and Assessing Regional Climate change in
High latitudes and the Arctic**
Grant agreement n° 242446

Ref: D4.2-y2
Date: 27/03/2012
Issue: 3
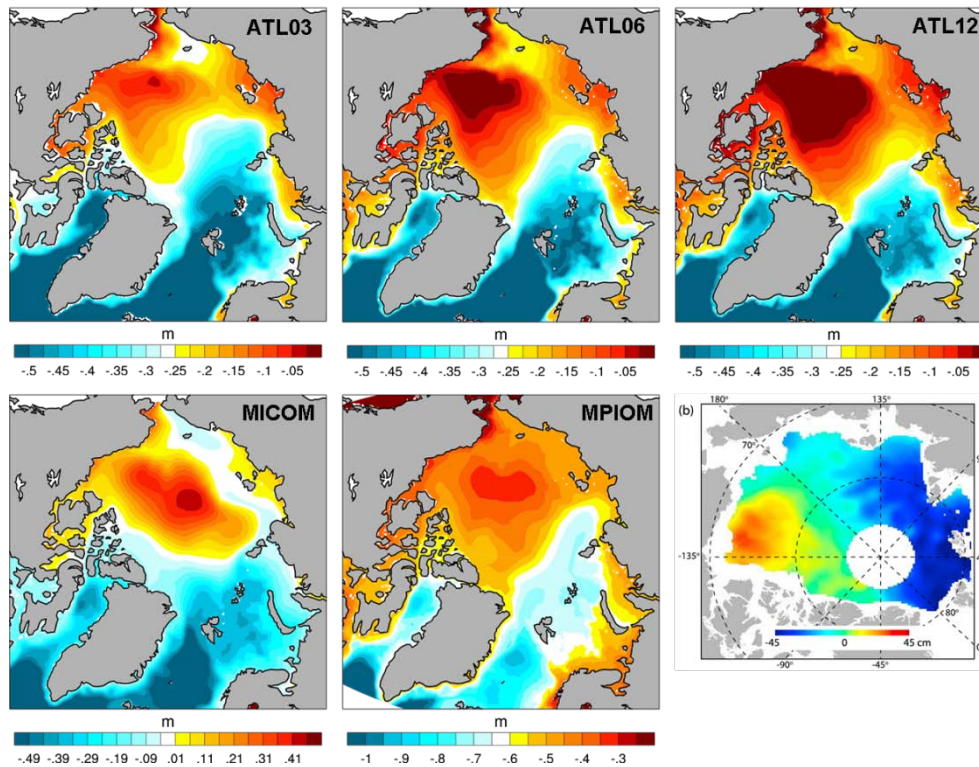
Figure 19. Mean SSH for the period 1970-2007 and Dynamical Ocean Topography estimate for 2004-2008 (Kwok et al., (2011). Note that the mean values of models and data are different

Surface ocean circulation: There are no direct measurements of the large scale surface ocean circulation in the Arctic Ocean, apart from large scale sea ice drift detected from ice buoys and satellite observations, and until recently there were no estimates of dynamical ocean topography for this region due to sea ice coverage and lack of detailed quantitative knowledge of the geoid. For this purpose Polar Pathfinder Daily 25 km EASE-Grid Sea Ice Motion Vectors data set (Fowler, 2003) is used; this combines satellite and buoy data and cover period from 1978 to 2006. Comparison of the simulated mean 1978-2006 surface currents with mean sea ice transport from satellite data for the same period shows that two main features of surface circulation of the Arctic Ocean - Beaufort Gyre and Transpolar Drift are relatively well represented in the simulations. All three runs locates the centre of the Beaufort Gyre close to the Canadian Coast, which is in good agreement with satellite data, as well as the Transpolar Drift from the East-Siberian and the Laptev Seas crossing the North Pole to the Fram Strait.

Focusing on the ATL12 run, it is seen that the model captures interannual variability as the recent trends in wind curl over the Amerasian Basin of the Arctic Ocean believed to cause intensification of the Beaufort Gyre. This leads to increase in Ekman pumping of the surface

MONARCH-A
MONitoring and Assessing Regional Climate change in High latitudes and the Arctic
Grant agreement n° 242446

Ref: D4.2-y2
Date: 27/03/2012
Issue: 3

fresh water to the interior of the ocean (Giles et al., 2012). The model is able to capture the corresponding intensification of the currents in Amerasian Basin (**Figure 20**).
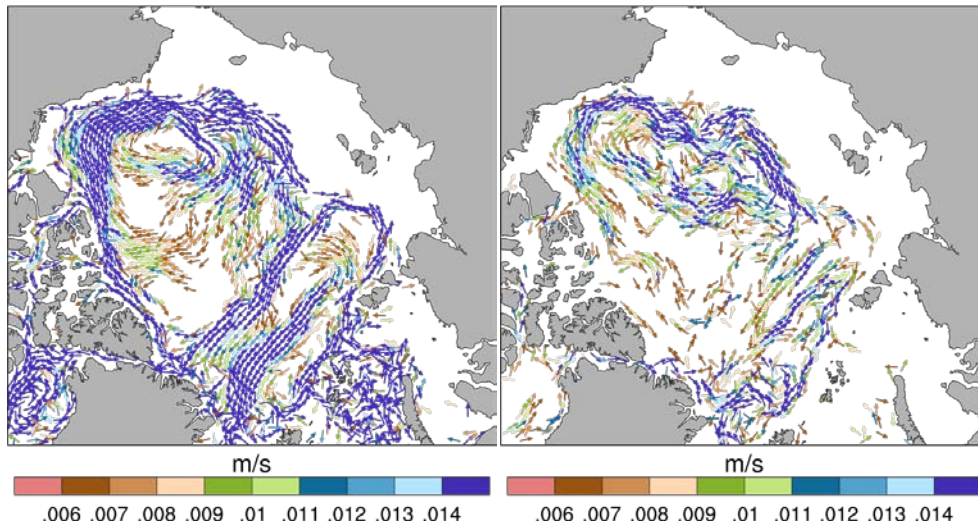
Figure 20. Currents at 105-172 m depth from ATL12 model simulation. Left: mean for 1970-2010, right: 2003-2010 anomaly relative to 1970-2010 mean.

During the same period **Figure 21** shows decrease in salinity in the Amerasian Basin during 2003-2010, that is especially strong between 80 to 200 meters. This feature is also described by the observations and well captured by the model.
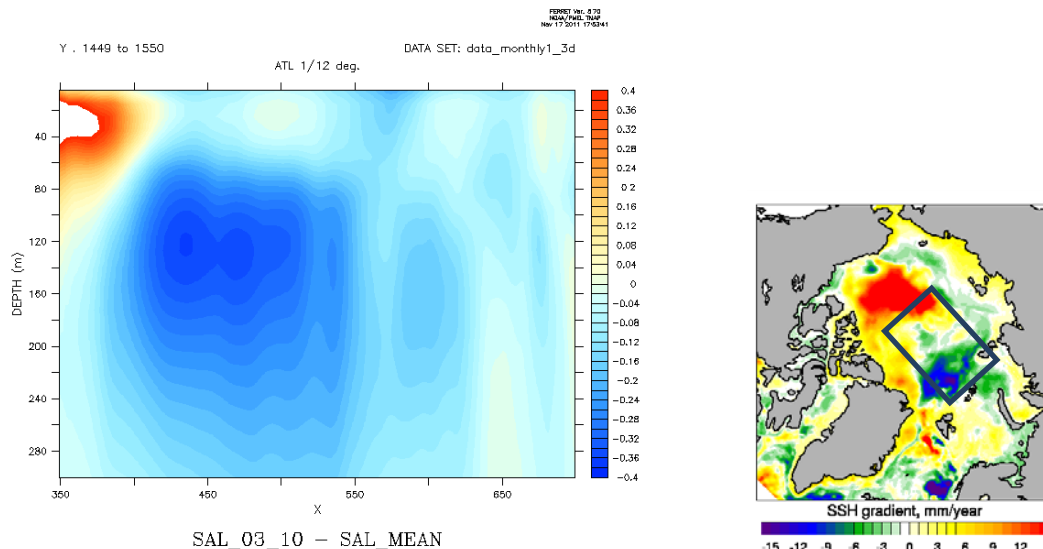
Figure 21. Mean 2003-2010 salinity anomaly (left) relative to 1970-2010 mean over transect across Amerasian Basin (map on the right).

MONARCH-A
MONitoring and Assessing Regional Climate change in High latitudes and the Arctic
Grant agreement n° 242446

Ref: D4.2-y2
Date: 27/03/2012
Issue: 3

3.4 Surface wind speed and direction

Satellite wind field retrievals for the high latitude and Arctic regions from the last 15-20 years are potentially a very valuable source of information for looking for instance at the role of extremes on seasonal-to-interannual scales. For validation, atmospheric fields include the continuously updated (and commonly used) NCAR/NCEP reanalysis product (Kalnay et al. 1996). These and the wind data from CERSAT/IFREMER, are intended as forcing fields for the oceanographic models. The CERSAT wind field with a resolution from 15 to 50 km is monitored using scatterometers since 1991, whereas NCAR/NCEP has 2.5^{o} resolution, although for several decades. Seasonal cyclone variability, storm track pathways and frequencies of extremes are assessed w.r.t to the location of sea ice edge, sea ice drift patterns and ocean circulation, and used further to assess the consequence for C02 partial pressure

A storm track algorithm based on satellite scatterometer datasets, dectecting all storm events (including hurricanes, typhoons and high latitude storms). **Figure 22** shows an example of a 3-months period storm detection. The properties are the storm position, the extension of the storm event, the storm center, the storm intensity and the maximum wind speed.

Storms can also be detected through wave-induced parameter, allowing to follow the trajectory of a storm and the corresponding values of the significant waves height values. The selection of the trajectories (Ardhuin *et al.* 2011) where one point exceed a value (for example 10 m in the 1998-2011 time series in **Figure 23**) highlights that storms can reach the high latitude oceans, during the winter.

Figure 22. Storm trajectories detected through the StormWatch algorithm for the period from June until September 2004

MONARCH-A
MONitoring and Assessing Regional Climate change in
High latitudes and the Arctic
Grant agreement n° 242446

Ref: D4.2-y2
Date: 27/03/2012
Issue: 3
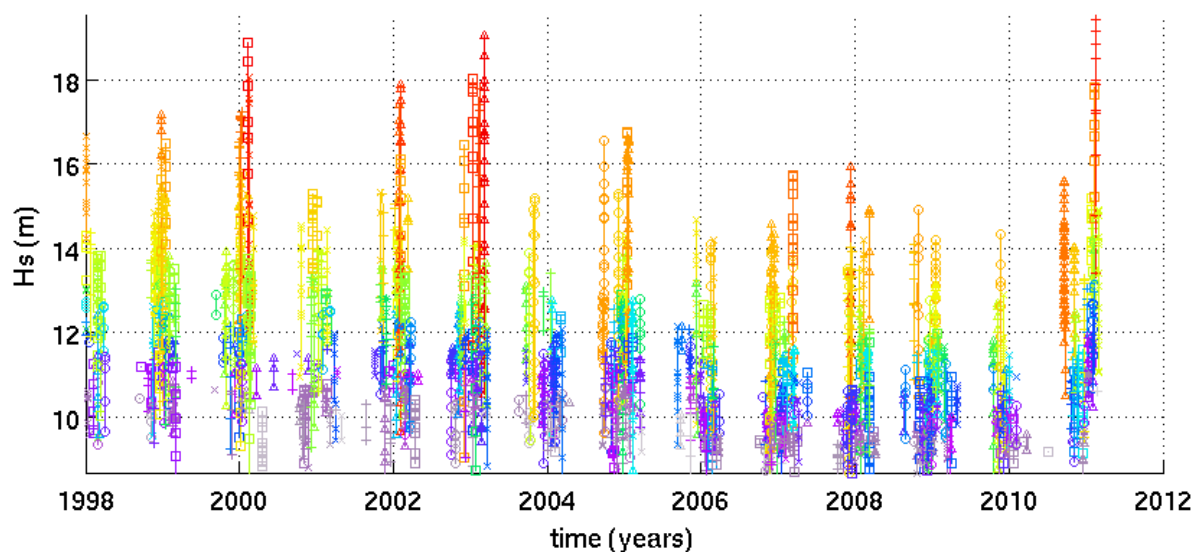
Figure 23. Time series of modeled significant waves height over a trajectory when one point exceeds 10 m, 1998-2011 period, latitude higher than 50°.

3.5   Sea ice drift

Important sources for sea ice data include MyOcean and the EUMETSAT OSI SAF. The observed sea ice parameters from satellites are primarily ice area, ice concentration and ice drift. Ice buoys also provide drift data at scattered locations across the Arctic, while moorings provide ice drift and thickness data in a few locations such as the Fram Strait. Ice thickness data for the Arctic Basin are obtained primarily from submarine cruises and scientific expeditions. Of particular relevance are the Russian expeditions, including the North Pole Drifting stations, which provide thickness and drift data over six decades starting in the 1930s. Additional data will be obtained from GLOBEICE and national archives, including those available in Canada and the US. Sea ice model will be used to bridge gaps in the incomplete ice data sets to produce 30-50 years time series

3.6   Sea ice extent, concentration

Sea ice extent (SIE) in models is compared with satellite data from Goddard Space Flight Center (GSFC) NASA Team algorithm (Cavalieri et al., 1996). We consider period from 1979 to 2007 and region to the north of 65N. Sea ice extent is defined as sum of the area of all gridpoints with sea ice concentrations greater than 15%. Seasonal cycle of the sea ice is well captured by all models, with MICOM comess closest to the satellite observations.

In general models are good in reproducing inter-annual variability (**Figure 24**). ATL model runs underestimates SIE, MPIOM overestimate it, while SIE values in MICOM are on average in good agreement with observations. Further experimenting shows that differences in the

MONARCH-A

MONitoring and Assessing Regional Climate change in High latitudes and the Arctic
Grant agreement n° 242446

Ref: D4.2-y2
Date: 27/03/2012
Issue: 3

deep ocean state practically do not have an effect on SIE, and it is determined mostly by surface atmospheric forcing and resolution.
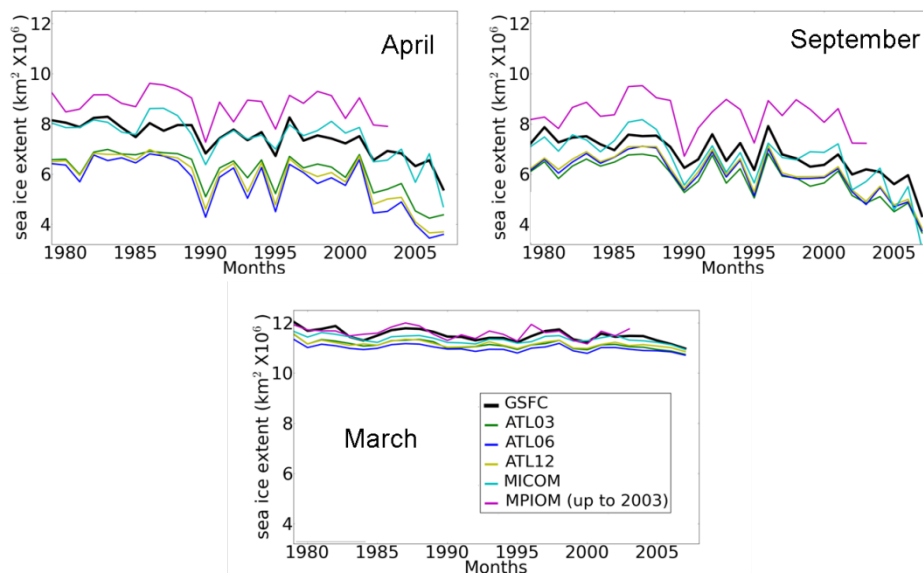
Figure 24. Inerannual variability of SIE for the period 1979-2007.

3.7 Sea ice thickness

Sea ice freeboard heights and dynamic topography of the Arctic Ocean observed from ICESat altimetry 2003-2008 release 28 are available in grids of resolution 0.1°x0.2°. The sea ice freeboard heights (**Figure 25**) show good correlation with backscatter values from QuikSCAT scatterometer data (Skourup, 2010). The freeboard (f) to thickness (t) conversion ($t = (1 + R) * f$) is debated in many papers and is highly variable (R = 1-10) depending on sea ice type, settings and snow conditions. Recent studies by Doble et al (2011) find a R-value of 3-3.5 for ICESat measurements. Thus, a key issue is to use the best conversion factor when computing ice thickness from ICESat freeboard heights. DTU Space is, furthermore, involved in the airborne measurements, which include overflights of ground teams working on the sea ice and direct underflights of CryoSat-2 over the Arctic sea ice (Skourup et al, 2011).

MONARCH-A
MONitoring and Assessing Regional Climate change in High latitudes and the Arctic
Grant agreement n° 242446

Ref: D4.2-y2
Date: 27/03/2012
Issue: 3
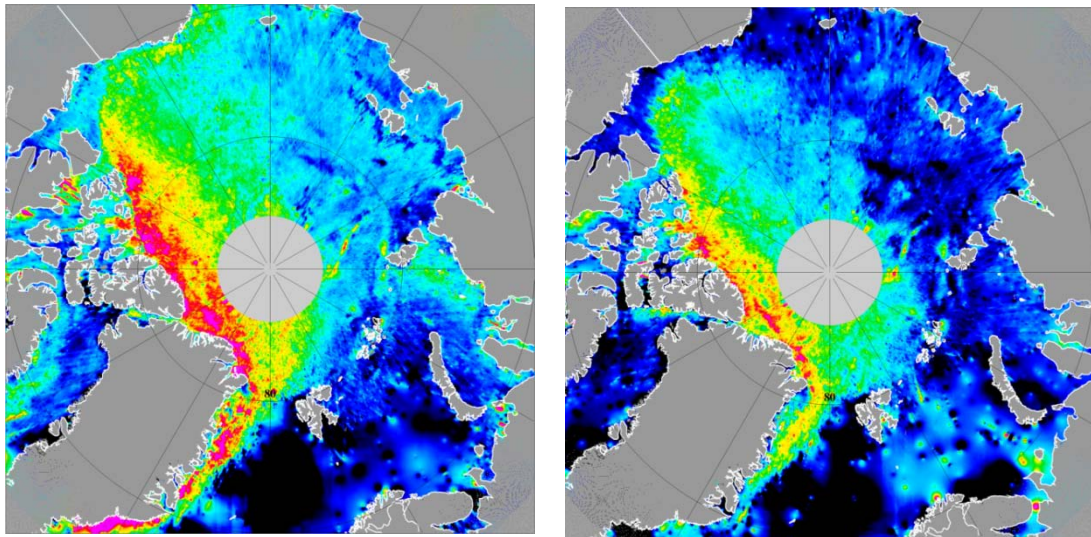
Figure 25. ICESat free board height from the periods October-November 2005 (left) and February-March 2006 (right).

Annual mean sea ice freeboard averages over the Arctic are shown in **Figure 26**. Overall, a decrease in the Arctic Ocean mean freeboard heights of approximately 15cm is observed, since the beginning of the ICESat observations in 2003. These are realistic values and can be explained by a combination of a decrease in the perennial sea ice extent together with a general decrease in the ice thickness due to an increased heating of the atmosphere and ocean.
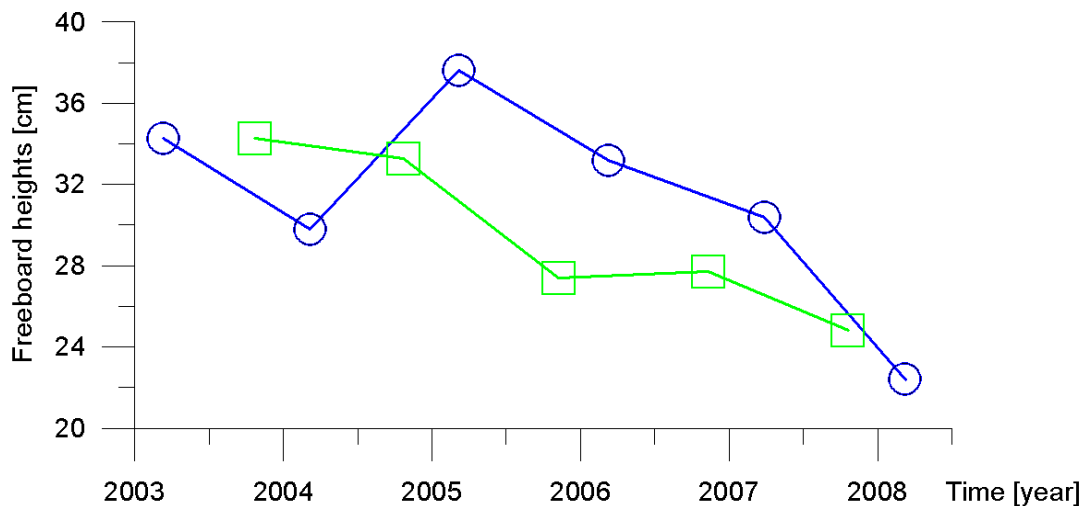
Figure 26. Annual mean sea ice freeboard heights averaged over the Arctic, showing a downward trend.

Ice thickness is one factor in determining ice flux. Combining with ice concentration and ice area flux one obtains sea ice volume flux. In Figure 27 the ice flux has been computed along

MONARCH-A
**MONitoring and Assessing Regional Climate change in
High latitudes and the Arctic**
Grant agreement n° 242446

Ref: D4.2-y2
Date: 27/03/2012
Issue: 3

79° N for six specific ICESat campaigns lasting approximately one month each from where good laser altimetry data are available. The result is comparable to Spreen et al., 2009, although somewhat on the high side and with considerable interannual variability.
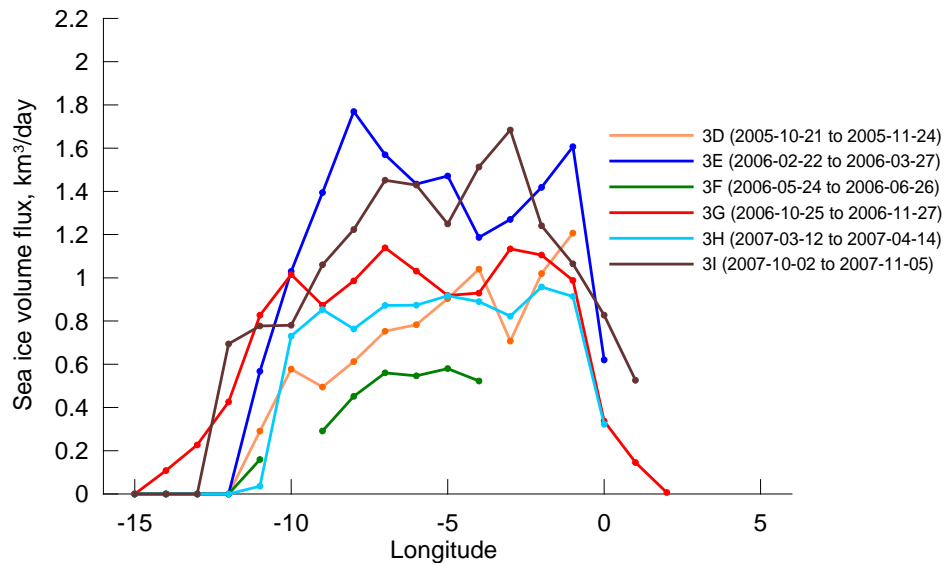
Figure 27. Sea ice volume flux [km3/day] southward across 79°N for six different ICESat campaigns. The quantity is derived from thickness data from NASA, ice concentration from passive microwave observations and area flux data from Kloster et al, (2009)

3.8   Sea surface temperature
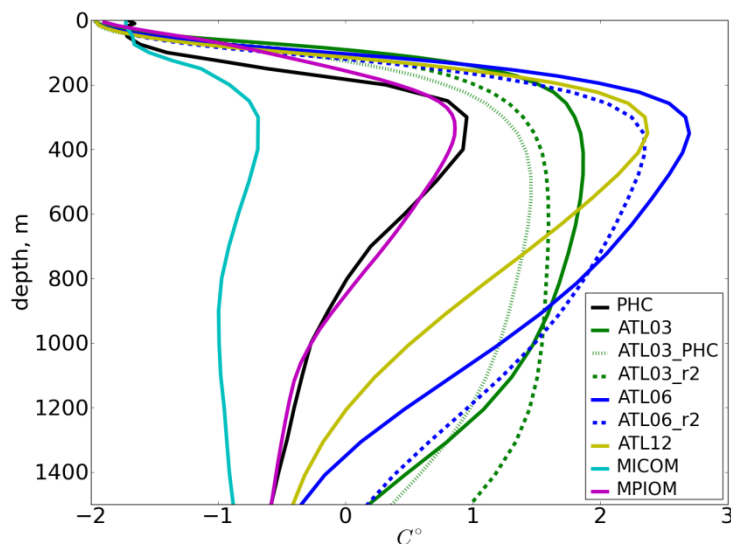
Figure 28. Vertical potential temperature profile averaged for Eurasian Basin of the Arctic ocean for winter (March, April, May) 1980-1989

MONARCH-A

**MONitoring and Assessing Regional Climate change in
High latitudes and the Arctic**
Grant agreement n° 242446

Ref: D4.2-y2
Date: 27/03/2012
Issue: 3

Both modelled and observed fields are considered. For comparison, the global Polar science center Hydrographic Climatology (PHC) (Steel, 2001) has been used for general comparison of modelled vs. observed water properties. The NISE data base (at NERSC) is also available for further analysis. Vertical temperature profiles (**Figure 28**) show that all models, except MICOM, reproduce intermediate Atlantic Water Layer (AWL, waters with temperatures above 0°C). Thickness of the AWL and its temperature is overestimated in ATL runs and is in good agreement in MPIOM run compared to PHC.

Mean temperature profile shows that ATL and MPIOM model runs are colder at the surface compared to PHC and that there is essentially no mixed layer presented. The MICOM model show well developed mixed layer with values close to the climatology. Ocean interior is warmer than PHC climatology in ATL runs, colder in MICOM model and in almost perfect agreement in MPIOM. Depth of the AW core in ATL06 and ATL12 runs is in the right position and the core itself is well developed. Repeated integrations (ATL03_r and ATL06_r) have lower temperatures above 1000 meters and higher temperatures below 1000 meters compared with runs started from climatology.

MONARCH-A
MONitoring and Assessing Regional Climate change in High latitudes and the Arctic
Grant agreement n° 242446

Ref: D4.2-y2
Date: 27/03/2012
Issue: 3

4. Changes in the marine carbon cycle

4.1 Surface ocean pCO_2 and air-sea CO_2 fluxes

To investigate the spatial distribution of pCO_2 seasonal complex algorithms have been developed so that pCO_2 could be determined from physical and biological variables available from models and satellites, one algorithm for winter (a) and one for summer (b) (Eq. 1a,b). The resulting mapped fields of surface ocean pCO_2 in the Barents Sea combined with atmospheric pCO_2 values from the Zeppelin station on Svalbard yield mapped fields of air-sea CO_2 flux in the Barents Sea for every month in 2007 (**Figure 29**) The Barents Sea is the only region with sufficient spatial and temporal data coverage, and 2007 is the year in which the full seasonal cycle in pCO_2 may be captured. pCO_2 data from R/V G.O.Sars in the Norwegian and Barents seas have also been analyzed, showing significant seasonal variability as expected at these latitudes (north of 55ºN), and there is also an expected annual increase in surface ocean pCO_2 in the years 2005-2007 due to an increasing anthropogenic CO_2 load in the atmosphere (see e.g. (Omar *et al.*, 2003)).

(1a) $fCO_2 = 0.4028 \pm 0.0529 \cdot SST + 19.4061 \pm 0.3615 \cdot SSS + 0.0051 \pm 0.0009 \cdot mld - 329.416 \pm 12.361$

(1b) $fCO_2 = -1.0979 \pm 0.1856 \cdot SST + 0.1725 \pm 0.0043 \cdot mld - 6.0448 \pm 0.644 \cdot Chl + 310.043 \pm 1.648$

As Fig. 1 shows, the calculated air-sea CO_2 fluxes are generally too high in winter and also in summer. The especially unrealistic fluxes for April and May could be due to these months being transition months when the spring bloom is at its strongest in the Barents Sea. It is in general more difficult to develop a working algorithm for periods of intense biological activity than for pre- and post-bloom periods. In addition there are strong intra-monthly changes during April and May.
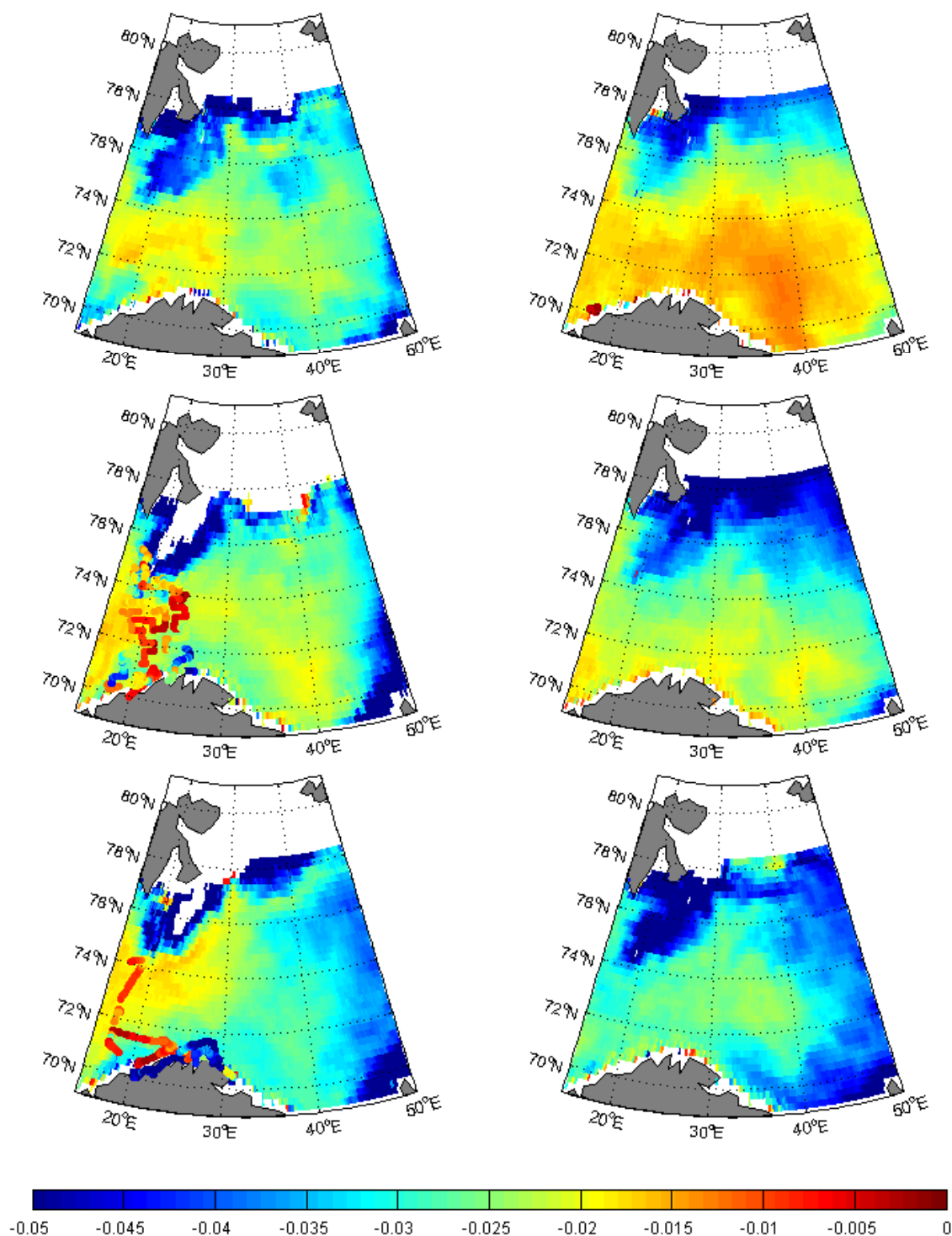
Figure 29. Monthly fields of air-sea CO_2 flux in the Barents Sea for winter 2007. The colored dots overlying the field show the observations in that given month. Top to bottom on the left hand side is winter (Jan-Mar) and top to bottom on the right hand side is fall (Oct-Dec).

More information on these data can be found in the report D3.1.3, www.socat.info, or contact the author, Siv K. Lauvset (siv.lauvset@gfi.uib.no). For details on the measurement technique, refer to Pierrot *et al.* (2009). In addition, the Year1 Synthesis Report for

MONARCH-A
MONitoring and Assessing Regional Climate change in High latitudes and the Arctic
Grant agreement n° 242446

Ref: D4.2-y2
Date: 27/03/2012
Issue: 3

Monarch-A contains good general information about how the marine carbon cycle is measured and the data sets available for different variables.

In order to illustrate the air-sea fluxes of CO_2 for the sub-Arctic and Arctic seas, we include here a previous result from the model BCM-C (**Figure 30**), where the regional contributions of different ocean basins to interior ocean transport of anthropogenic carbon and transport across the air-sea interface over time have been quantified (Tjiputra *et al*, 2010b).
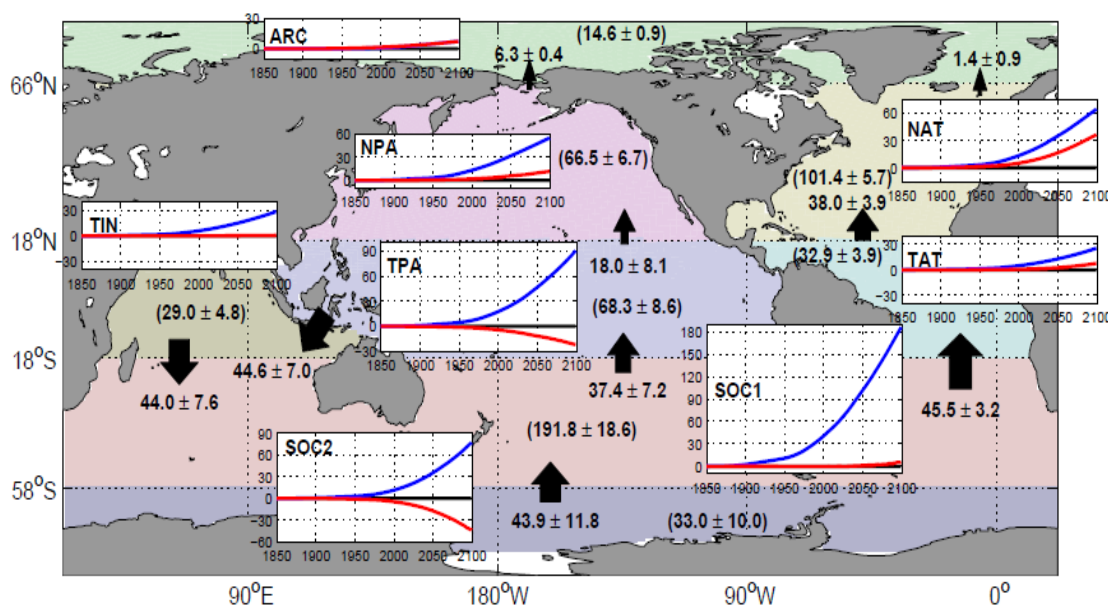
Figure 30. Accumulated fluxes of anthropogenic carbon C_{ant}) from the atmosphere to the sea (blue-line) and compared to horizontal fluxes (red-line) into different ocean regions during 1850–2099 period. Negative values indicate out of the region and vice versa. All fluxes are given in (PgC). Arrow-number pairs show accumulated transport fluxes of C_{ant} between regions for the period 1850-2099. Numbers inside parenthesis indicate the storage of C_{ant} in the respective region at the end of experiment period. (Source: Tjiputra et al., 2010b)

This analysis confirms earlier studies that the Arctic Ocean is only a minor uptake area for human produced CO_2. Nevertheless, studies of the Arctic are essential, e.g. due to the fact that the change of pH and carbonate saturation ("ocean acidification") is most pronounced in high latitude surface waters. A new revised spin-up of the standalone coupled physical-biogeochemical ocean model MICOM-HAMOCC has been carried out, and towards the end of the project new model hindcast for the past ca. 50 years is planned. For these runs, ocean only models forced by atmospheric synoptic data and prescribed (observed) atmospheric CO2 partial pressure will be used, as a fully coupled Earth system model will produce its own weather and interannual variability, which is incompatible with the the real variations for respective calendar years.

MONARCH-A

**MONitoring and Assessing Regional Climate change in
High latitudes and the Arctic**
Grant agreement n° 242446

Ref: D4.2-y2
Date: 27/03/2012
Issue: 3

3.2 pCO2 atmosphere

Atmospheric CO_2 partial pressure [µatm] (or atmospheric CO_2 volume mixing ratio [ppmv]) can be simulated with the ocean biogeochemical model versions used in MONARCH-A if their atmospheric gas reservoir is kept as free floating. In most re-analyses, however, the atmospheric CO_2 partial pressure is prescribed according to observations. For *prognostic* climate type ocean models short term variations such as seasonal changes and spatially different seasonal amplitudes of atmospheric CO_2 are of minor importance, due to the long equilibration time for the surface ocean with atmospheric CO_2 (ca. 200 days, Sarmiento and Gruber, 2006) as well as due to the fast intra-hemispheric (few weeks) and inter-hemispheric (1 year) tropospheric mixing times. For atmospheric inverse studies (not carried out within MONARCH-A) short term spatio-temporal variability would be critically important for assessing land-air and ocean-air CO_2 fluxes for the sake of e.g. CO_2 emission control.
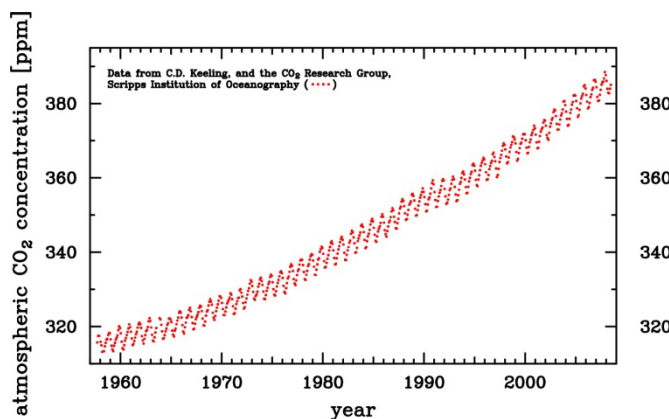
Figure 31. Mauna Loa atmospheric CO_2 record after Keeling et al. (2009).

State and variability: Today there is no steady-state in atmospheric CO_2 concentrations as seen by the strong increase that started in the early decades of the 19th century (e.g. Etheridge et al., 1998; Neftel et al., 1994). During the past 650 kyr, CO_2 varied within a limit of 180-300 ppmv (Siegenthaler et al., 2005). High quality measurements exist since 1957/58 (Keeling et al., 2001, **Figure 31**). Since then the CO_2 data data base has increased steadily, also supplemented with aircraft measurements.

The annual mean CO_2 is increasing monotonically over the entire instrumental CO_2 record and is attributed to the anthropogenic CO_2 emissions (fossil fuel burning, cement manufacturing, land use). The seasonal amplitude is a result of the "breathing" of the land-biosphere and that most land carbon reservoirs are located in the Northern hemisphere. Interannual variability occurs due to short term climatic fluctuations (e.g., ENSO, NAO, SAM) and variations in human produced CO_2 emssions (e.g., recent financial crisis, Peters et al., 2012).

State-of-the-art data product for atmospheric CO_2 measurements is GLOBALVIEW of the U.S. NOAA ESRL (http://www.esrl.noaa.gov/gmd/ccgg/globalview/CO2/CO2_intro.html). It is an integration of available high quality measurements (stationary surface and tower sites, moving ship and aircraft sites) into a consistent data base with best possible spatial

MONARCH-A

**MONitoring and Assessing Regional Climate change in
High latitudes and the Arctic**
Grant agreement n° 242446

Ref: D4.2-y2
Date: 27/03/2012
Issue: 3

coverage ; for more details see
http://www.esrl.noaa.gov/gmd/ccgg/globalview/gv_goals.html and Masarie and Tans (1995).

Highest quality atmospheric CO_2 measurements can be obtained from
http://scrippsCO$_2$.ucsd.edu/data/atmospheric_CO$_2$.html. This data base (Keeling et al., 2001,
2005) covers the longest time series (including the Mauna Loa measurements) and a wide
latitudinal range (from Alert, NWT, Canada 82.3 N 62.3 W, to South Pole 90.0 S) (**Figure 31**).

3.2.1   Ocean color

Based on satellite derived ocean color primary production rates and associated multi-year
trends are separately established for the ice-free pelagic area of the Arctic Basin and for
shelf seas. The inorganic carbon input due to blooms of coccolithophore E. huxleyi is also
assessed, using MODIS processed with the NIERSC dedicated algorithm and columnar
concentration of inorganic carbon is being assessed using the TOPAZ MLD data.

Trends of PP interannual variations (monthly mean values) as obtained through application
of the Behrenfeld (1997, 2005) models/algorithms to SeaWiFS data processed with the
NASA GSM code were plotted for the time period 1998-2010 are nearly zero indicating
either no or very insignificant dynamics. However, when the cloudiness effect is properly
taken into account, some positive trend is seen over the decade of satellite observations
(**Figure 32**), consistently between all three algorithms.
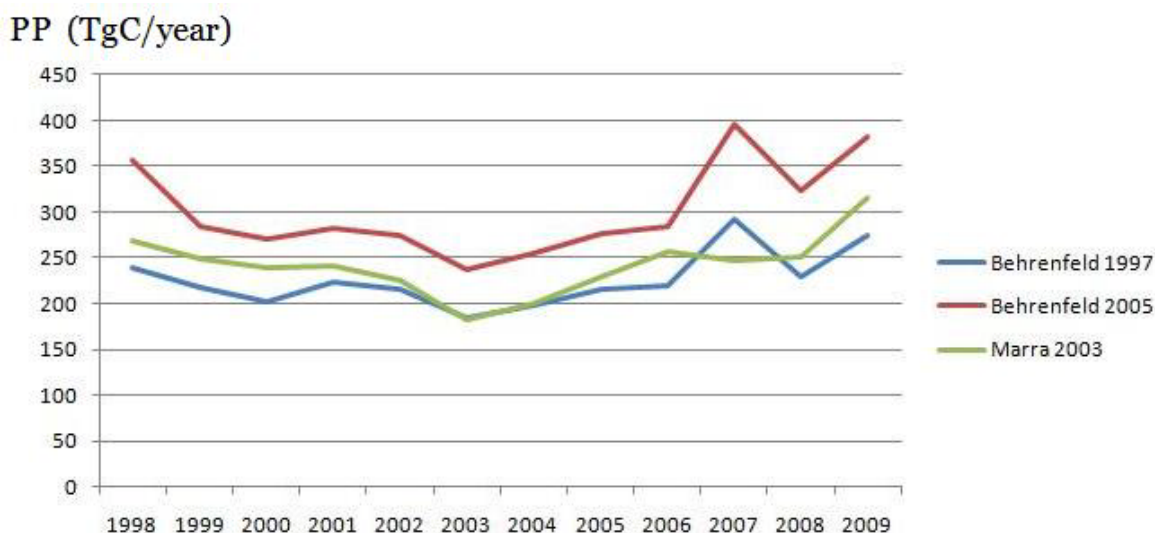
Figure 32. Annually averaged Primary Production (TgC/year) versus time (years)

MONARCH-A

MONitoring and Assessing Regional Climate change in High latitudes and the Arctic
Grant agreement n° 242446

Ref: D4.2-y2
Date: 27/03/2012
Issue: 3

3.3   Inorganic carbon production.

Satellite-based (Level 3 MODIS data)assessments of inorganic carbon production by *E. huxleyi* in the Arctic Ocean have also been performed during 2002-2010, indicating that it was generally declining as a result of a declining bloom intensity and spatial extent. Jointly, SST and PAR within the bloom areas showed a decreasing tendency. Furthermore, a declining North Atlantic Oscillation suggests that the established decline in inorganic carbon production due to *E. huxleyi* blooms is mostly controlled by the decrease in advection of *E. huxleyi* seeds from the European marine areas lying to the south of the Polar Circle. It is known that the seeding process is important for the beginning of a rapid and extensive growth of this alga. Declining SST and PAR also contributed to a general decrease in inorganic carbon production.

Figure 33 and **Figure 34** shows the monthly dynamics in inorganic carbon production per m^2, respectively, in the Barents Sea and the entire Arctic, respectively, over 2002- 2010.
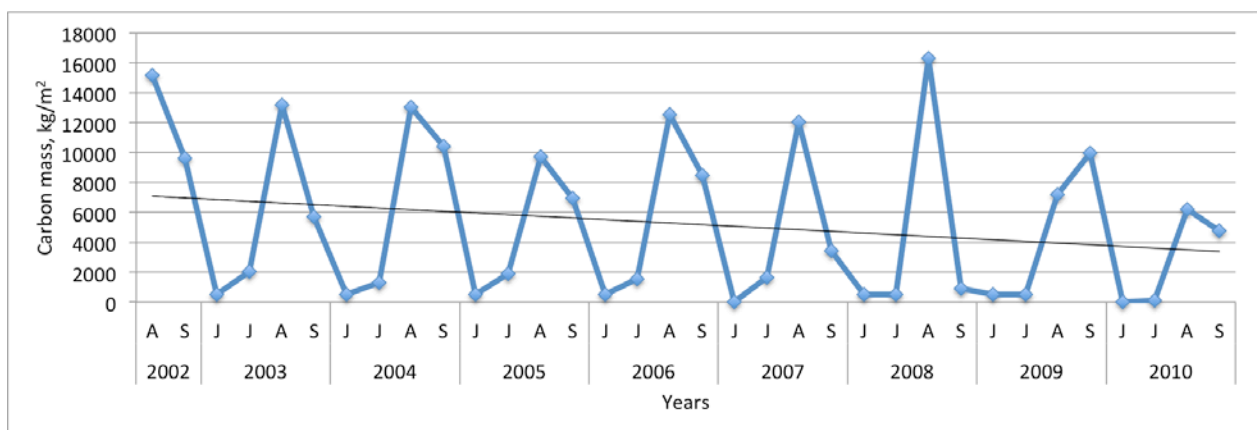
Figure 33. Monthly and interannual dynamics in inorganic carbon production per m^2 in the Barents Sea over 2002-2010.
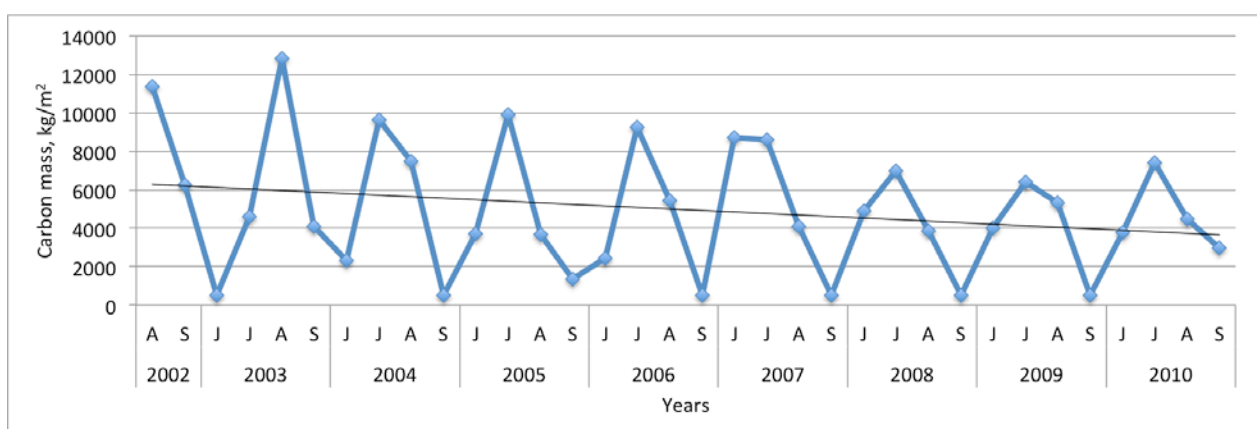
Figure 34. Monthly and interannual dynamics in inorganic carbon production per m^2 in the entire Arctic over 2002-2010.

MONARCH-A
MONitoring and Assessing Regional Climate change in
High latitudes and the Arctic
Grant agreement n° 242446

Ref: D4.2-y2
Date: 27/03/2012
Issue: 3

5. Conclusion

A synthesis status of the data analysis and modelling work for the 11 MONARCH-A Essential Climate Variables (ECVs) is provided. This forms a basis for informing the GMES core service accordingly. The compilation of data sets and results after 2 years provides new and more accurate characterization of the state and variability of river discharge, snow cover and snow water equivalent, permafrost extent and seasonal variability of frozen ground; sea level and Greenland ice sheet mass loss, ocean currents and sea ice drift as well as ocean mass and heat transport, CO_2 partial pressure, and near surface wind field.

From these results, trends in several parameters are already emmanent, at least for the last 10-30 years, but forthcoming synthesis will address trends and variability more in-depth in order to establish a more comprehensive quantitative understanding of the climate changes in the high latitude and Arctic region over the last 50-60 years, including

- New and better quantification of mutual forcing and feedback mechanisms of the high latitude and Arctic climate system
- New knowledge and support to the attribution of the causes of high latitude climate change; interannual-to-decadal high latitude climate prediction; understanding of the connections between global and regional climate change.

In particular the data sets and reanalyses include:

(Land:)

- Comparison of several state-of-the-art land surface models of **land cover and fires** with comprehensive data sets and modifications to better represent observed data properties
- Comparison of several state-of-the-art land surface models of **snow water equivalent** and **river discharge** versus comprehensive data sets and introduction of a simple delay model to give better agreement with monthly runoff
- New estimates of **discharges** from major Arctic **rivers** using a combination of altimetric observations of water level and historical in situ data on river discharge, also including lake levels
- 22 years of satellite derived **snow** extent and start and end dates of snow cover; new in situ observations of snow properties (depth, density etc) to enable calculation of satellite-derived snow water equivalent fields
- A reference **permafrost** map
- A 16 years time series of altimetry based Greenland **Ice Sheet** elevations to be compared with recent gravimetry based data sets

(Ocean:)

- **Sea level** estimates from evaluated ocean multi-model reanalyses, as well as reconstructions back to 1950 based on combining hydrography, altimetry and tidal gauge measurements
- **Ocean currents** based on model simulation from several models that have been evaluated

MONARCH-A
MONitoring and Assessing Regional Climate change in High latitudes and the Arctic
Grant agreement n° 242446

Ref: D4.2-y2
Date: 27/03/2012
Issue: 3

- Satellite **wind field** retrievals from the last 15-20 years validated against reanalysis products
- **Sea ice drift** from sea ice models in combination with satellite and in situ buoys and drift station measurements over the last 30-50 years
- **Sea ice extent** estimates from evaluated ocean multi-model reanalyses, as well as remote sensing data
- **Sea ice thickness.** Ice freeboard measurements from ICEsat, QuickScat and preliminary CryoSat-2 have been compared
- **Sea surface temperature** distribution from evaluated models and public domain data bases

(Marine carbon cycle:)

- **Ocean surface pCO2:** A comprehensive data base on sea surface CO_2 partial pressure and related carbonate system parameters, together with recent ship observations of **atmospheric pCO2** has been provided**.**
- A complete **ocean carbon system model data set** for the pre-industrial ocean was established through a spin-up of the ocean only coupled physical-biogeochemical ocean model MICOM-HAMOCC. This run provides the basis for hindcats using prescribed atmospheric CO2 and synoptic atmospheric forcing from re-analyses for the past 50 years.
- **Ocean color** and primary productivity estimates for the Arctic Ocean based on remotely sensed data. Differentiated between coastal and open areas and using respectively extended algorithms. Separate estimate for production of particulate inorganic carbon (or calcium carbonate $CaCO_3$).

6. Appendix

ECV	Data sources			Algorithms and Models	Derived information product
	Satellite	**In-situ**	**Complement**		
Vegetation cover	Optical, active microwaves	Limited and spotty	GLOBCOVER, G-2, GLC-2000, MODIS products including VCF	SDGVM, BCM, NorESM, Orchidee, JULES	Fraction of Plant Functional Type per model grid-cell
Fire	Optical and infrared	Limited and spotty	MODIS Collection 5, GBA-2000, GLOBCARBON, MODIS FRP, SEVIRI FRP	SDGVM, BCM, NorESM, Orchidee, JULES	Burnt area and carbon emissions
River discharges	Radar altimeters	Flow gauges - Global Runoff Data Centre		Discharge from water level estimates	Contribution to freshwater runoff
Snow cover	Passive and active microwaves	Spotty station observations of snow cover and depth	G-2 GLOBECOVER	Snow depth retrieval algorithm; conversion to snow water equivalent	Contribution to freshwater runoff, Impact on albedo,

MONARCH-A

MONitoring and Assessing Regional Climate change in High latitudes and the Arctic

Grant agreement n° 242446

Ref: D4.2-y2
Date: 27/03/2012
Issue: 3

ECV	Data sources			Algorithms and Models	Derived information product
	Satellite	**In-situ**	**Complement**		
Permafrost	Passive and active microwaves	Rare and spotty	G-2 GLOBECOVER	Permafrost-soil-snow-atmosphere module	Permafrost maps
Ice sheets and glaciers	Passive and active microwaves, GRACE	Selected repeat ground profiling	Database of aircraft altimeter observations along selected profiles		,Mass balance change; Contribution to sea level and freshwater runoff
Sea level	Altimetry,	Tide gauges, hydrography, GNSS	MYOCEAN, GLOSS, PSMSL, SALTO/DUACS NISE data base	GECCO BCM, NorESM GIA models	High latitude and Arctic Ocean regional sea level variations
Current	Altimetry for geostrophic current,	Very limited north of 65 degrees N	MYOCEAN drifters, moorings	GECCO, MICOM, BCM, NorESM	Heat and volume transports
Ocean color	Imaging spectrometers	Limited data on marine biology primary production; nearly no data on export production; selected data on water column biogeochemistry (carbon, alkalinity, nutrients, oxygen) exist	MYOCEAN GLOBCOLOR, CZCS, SeaWIFS, MODIS, MERIS	HAMOCC coupled to MICOM	Primary production of POC (particulate organic carbon) and possibly PIOC (particulate inorganic carbon) and its influence on CO_2 fluxes
Sea ice drift	Passive and active microwaves	Ice buoys	MYOCEAN GLOBEICE	GECCO MICOM	Transport across straights. Contribution to freshwater

MONARCH-A

**MONitoring and Assessing Regional Climate change in
High latitudes and the Arctic**
Grant agreement n° 242446

Ref: D4.2-y2
Date: 27/03/2012
Issue: 3

ECV	Data sources			Algorithms and Models	Derived information product
	Satellite	**In-situ**	**Complement**		
				BCM, NorESM	
Surface wind speeds and direction	Passive microwaves, scatterometer	Ice buoys, coastal stations	CERSAT ECMWF NCEP	GECCO, MICOM, BCM, NorESM	Wind climatology, storm tracks, surface stress, curl
Partial pressure CO2 ocean	Not possible direct, wind speed from satellites used	Very limited data, from research vessel and VOS	SOCAT (surface ocean), CARINA (3D), CARBOOCEAN EPOCA	HAMOCC coupled to MICOM	Air-sea CO2 fluxes, acidification
Partial pressure CO2 atmosphere	Aeroplane and possibly satellite measurements	Flask measurements and continuous measurements	NOAA, SIO, CSIRO, GOSAT (2009)	HAMOCC slab atmosphere	CO2 and its impact on radiation
Sea ice extent, concentration,	Passive and active microwaves,		MYOCEAN OSI-SAF CM-SAF GLOBICE	GECCO, MICOM, BCM, NorESM	Regional high latitude sea ice climatology, impact on albedo
Sea ice thickness	Radar and laser altimetry	Spotty station observations	MYOCEAN	GECCO, MICOM, BCM, NorESM	
Sea surface temperature	Passive microwaves, IR,	XBT lines, VOS	MYOCEAN GHRSST, OSI-SAF, CM-SAF	GECCO, MICOM, BCM, NorESM	High latitude and Arctic SST fields in consistence with sea ice extent and heat fluxes

Table 1: Essential Climate Variables, their observation type, specific data source and derived products (white rows). The ECVs in the yellow rows will be formed by synthesizing available datasets and casting them into forms suitable for exploitation by models. The ECVs in the brown rows will be pulled from existing archives, but not refined.

	MONARCH-A	Ref: D4.2-y2
	MONitoring and Assessing Regional Climate change in High latitudes and the Arctic	Date: 27/03/2012
	Grant agreement n° 242446	Issue: 3

7. References

Antonov, J. I., S. Levitus, T. P. Boyer, M. E. Conkright, T. D. O'Brien, and C. Stephens, 1998: World Ocean Atlas 1998 Vol. 1: Temperature of the Atlantic Ocean. NOAA Atlas NESDIS 27, 166 pp.

Arctic Climatology Project. 1997. Environmental Working Group joint U.S.-Russian atlas of the Arctic Ocean - winter period. Edited by L. Timokhov and F. Tanis. Ann Arbor, MI: Environmental Research Institute of Michigan in association with the National Snow and Ice Data Center. CD-ROM.

Arctic Climatology Project. 1998. Environmental Working Group joint U.S.-Russian atlas of the Arctic Ocean - summer period. Edited by L. Timokhov and F. Tanis. Ann Arbor, MI: Environmental Research Institute of Michigan in association with the National Snow and Ice Data Center. CD-ROM.

Ardhuin F., J. Hanafin, Y. Quilfen, B. Chapron, P. Queffeulou, M. Obrebski, J. Sienkiewicz, D. Vandemark calibration of the IOWAGA global wave hindcast (1991–2011) using ECMWF and CFSR winds," in Proceedings, 12th Int. Workshop of Wave Hindcasting and Forecasting, Hawaii, 2011.

Beer, B , M. Reichstein , E. Tomelleri , P Ciais , M. Jung, N. Carvalhais , C. Rödenbeck , M. A. Arain , D. Baldocchi , G. B. Bonan , A. Bondeau , A. Cescatti , G. Lasslop , A. Lindroth , M. Lomas, S. Luyssaert , H. Margolis , K. W. Oleson , O. Roupsard , E. Veenendaal , N Viovy , C. Williams , F. I. Woodward, D. Papale, Terrestrial Gross Carbon Dioxide Uptake: Global Distribution and Covariation with Climate, Science, doi: 10.1126/science.1184984.

Biancamaria, S., N. Mognard, A. Boone, M. Grippa, A. Josberger, 2008, "A satellite snow multi-year average derived from SSM/I for the high latitude regions", Remote Sensing of Environment, vol. 112, 2447-2568.

Boone, A., N. Mognard, B. Decharme, H. Douville, M. Grippa, K. Kerrigan, 2006, "The impact of simulated soil temperatures on the estimation of snow depth over Siberia from SSM/I compared to a multi-model climatology", Remote Sensing of Environment ,vol. 101, 482-494.

Boyer, T., Levitus, S., Garcia, H., Locarnini, R., Stephens, C. and coauthors. 2005. Objective analyses of annual, seasonal, and monthly temperature and salinity for the World Ocean on a 0.25◦ grid. Int. J. Climatol. 25(7), 931–945.

Cavalieri, D., C. Parkinson, P. Gloersen, and H. J. Zwally, 1996, updated 2008: Sea ice concentrations from Nimbus-7 SMMR and DMSP SSM/I passive microwave data 1980–1999. National Snow and Ice Data Center, digital media. [Available online at http://nsidc.org/data/nsidc-0051.html.]

http://cdiac.ornl.gov/trends/CO$_2$/sio-mlo.html

Chambers, D.P. (2006), Evaluation of New GRACE Time-Variable Gravity Data over the Ocean. Geophys. Res. Lett., 33(17), LI7603.

Chang, A. T. C., J. L. Foster, D. K. Hall, 1987, "Nimbus-7 SMMR derived global snow cover parameters", Annals of Glaciology, 9, 39-44.

Chylek, P., C. K. Folland G. Lesins and M. K. Dubey (2010), Twentieth century bipolar seesaw of the Arctic and Antarctic surface air temperatures, Geophys. Res. Lett., 37, L08703, doi:10.1029/2010GL042793.

Duguay C. , Kang K-K, Kouraev A., Mercier F. Estimation of ice thickness on large lakes from passive microwave and radar altimeter data. EGU-2010, Vienna.

Etheridge, D. M., L.P. Steele, R.L. Langenfelds, R.J. Francey, J.-M. Barnola and V.I. Morgan, 1998, Historical CO_2 records from the Law Dome DE08, DE08-2, and DSS ice cores. In Trends: A Compendium of Data on Global Change. Carbon Dioxide Information Analysis Center, Oak Ridge National Laboratory, U.S. Department of Energy, Oak Ridge, Tenn., U.S.A., http://cdiac.ornl.gov/trends/CO2/lawdome.html

Foster, D.J. and R.D. Davy, 1988, "Global Snow Depth Multi-Year Average", USAFETAC/TN-88/006. Illinois: Scott Air Force Base. 48 pp.

Forsberg, R., V. R. Barletta, L. S. Sørensen: Monarch-A D2.3.3 Gridded time series of GRACE-based Greenland mass changes, September 2011

Gao, Y., 2004. Simulating transport of non-Chernobyl 137Cs and 90Sr in the north Atlantic–Arctic region. Journal of Environmental Radioactivity 71 (1), 1-16.

Giles, K. A., Laxon, S. W., Ridout, A. L., Wingham, D. J., Bacon, S., Jan. 2012. Western arctic ocean freshwater storage increased by wind-driven spin-up of the beaufort gyre. Nature Geosci advance online publication. URL http://dx.doi.org/10.1038/ngeo1379

Grippa, M., N. Mognard, T. Le Toan, E.G Josberger, 2004, "Siberia snow depth climatology derived from SSM/I data using a combined dynamic and static algorithm", Remote Sensing of Environment, vol. 93, 30-41.

Hátún, H., Sandø, A. B., Drange, H., Hansen, B., Valdimarsson, H., Sep. 2005. Influence of the Atlantic subpolar gyre on the thermohaline circulation. Science 309 (5742), 1841-1844.

Holland, D., R. H. Thomas, B. De Young, M. H. Ribergaard and B. Lyberth (2008), Acceleration of Jakobshawn Isbrae triggered by warm subsurface ocean waters, Nature Geosciences, vol. 1, 659-664, doi:10.1038/ngeo316.

Holloway, G., Dupont, F., Golubeva, E., Häkkinen, S., Hunke, E., Jin, M., Karcher, M., Kauker, F., Maltrud, M., Morales Maqueda, M. A., Maslowski, W., Platov, G., Stark, D., Steele, M., Suzuki, T., Wang, J., Zhang, J., Mar. 2007. Water properties and circulation in arctic ocean models. Journal of Geophysical Research 112 (C4), C04S03+.

Fowler, C. 2003, updated 2008. Polar Pathfinder Daily 25 km EASE-Grid Sea Ice Motion Vectors. Boulder, Colorado USA: National Snow and Ice Data Center. Digital media.

Huntingford, C, B. B. B. Booth , S. Sitch , N. Gedney , J. A. Lowe , S. K. Liddicoat , L. M. Mercado , M. J. Best , G. P.Weedon , R. A. Fisher, M. R. Lomas, P. Good , P. Zelazowski, A. C. Everitt , A. C. Spessa and C. D. Jones , IMOGEN: an intermediate complexity model to evaluate terrestrial impacts of a changing climate. Geosci. Model Dev., 3, 679-687, 2010 www.geosci-model-dev.net/3/679/2010/ doi:10.5194/gmd-3-679-2010.

Josberger, E.G. and N. Mognard, 2002, "A passive microwave snow depth algorithm with a proxy for snow metamorphism", Hydrological Processes, vol. 16, 15557-1586. doi:10.1002/hyp.1020.

Jutterström, S., Anderson, L.A., Bates, N.R., Bellerby, R., Johannessen, T., Jones, E.P., Key, R.M., Lin, X., Olsen, A., Omar, A., 2009. Arctic Ocean data in CARINA. Earth Syst. Sci. Data 2 (281-308).

MONARCH-A

MONitoring and Assessing Regional Climate change in High latitudes and the Arctic
Grant agreement n° 242446

Ref: D4.2-y2
Date: 27/03/2012
Issue: 3

Kalnay, E., Kanamitsu, M., Kistler, R., Collins, W., Deaven, D., Gandin, L., Iredell, M., Saha, S., White, G., Woollen, J., Zhu, Y., Leetmaa, A., Reynolds, B., Chelliah, M., Ebisuzaki, W., Higgins, W., Janowiak, J., Mo, K. C., Ropelewski, C., Wang, J., Jenne, R., Joseph, D., Mar. 1996. The NCEP/NCAR 40-Year reanalysis project. Bulletin of the American Meteorological Society 77 (3), 437-471.

Karcher, M., Kauker, F., Gerdes, R., Hunke, E., Zhang, J., Apr. 2007. On the dynamics of atlantic water circulation in the arctic ocean. Journal of Geophysical Research 112 (C4), C04S02+.

Karcher, M. J., R. Gerdes, F. Kauker and C. Koberle (2003), Arctic warming: evolution and spreading of the 1990s warm event in the Nordic seas and the Arctic Ocean, J. Geophys. Res., 108, C2, 3034, doi:10.1029/2001JC001265.

Keeling, C. D., S. C. Piper, R. B. Bacastow, M. Wahlen, T. P. Whorf, M. Heimann, and H. A. Meijer, Exchanges of atmospheric CO_2 and $13CO_2$ with the terrestrial biosphere and oceans from 1978 to 2000, 2001, I. Global aspects, SIO Reference Series, No. 01-06, Scripps Institution of Oceanography, San Diego, 88 pages.

Keeling, C. D., S. C. Piper, R. B. Bacastow, M. Wahlen, T. P. Whorf, M. Heimann, and H. A. Meijer, 2005, Atmospheric CO_2 and $^{13}CO_2$ exchange with the terrestrial biosphere and oceans from 1978 to 2000: observations and carbon cycle implications, pages 83-113, in "A History of Atmospheric CO_2 and its effects on Plants, Animals, and Ecosystems", editors, Ehleringer, J.R., T. E. Cerling, M. D. Dearing, Springer Verlag, New York.

Keeling, R.F., S.C. Piper, A.F. Bollenbacher and J.S. Walker, 2009, Atmospheric CO_2 records from sites in the SIO air sampling network. In Trends: A Compendium of Data on Global Change. Carbon Dioxide Information Analysis Center, Oak Ridge National Laboratory, U.S. Department of Energy, Oak Ridge, Tenn., U.S.A. doi: 10.3334/CDIAC/atg.035

Key, R.M., Tanhua, T., Olsen, A., Hoppema, M., Jutterström, S., Schirnick, C., Van Heuven, S., Kozyr, A., Lin, X., Velo, A., Wallace, D.W.R., Mintrop, L., 2010. The CARINA data synthesis project: introduction and overview. Earth Syst. Sci. Data 2, 105-121.

Khvorostovsky, K. Merging and analysis of elevation time series over Greenland Ice Sheet from satellite radar altimetry. IEEE, IEEE Trans. Geosci. Remote Sensing, 2011, submitted revision.

K. Khvorostovsky: Monarch-A D2.3.1 Time series of satellite altimetry height changes of the Greenland ice sheet, year since 1992 expressed as height change grids, September 2011

Kirpotin S., Polishchuk Y., Pokrovsky O., Kouraev A, Bryksina N., Sugaipova A., Zakharova E., Shirokova L., Kolmakova M., Manassypov R., Dupre B. 2010. Vegetation Response on Climatic Changes in West-Siberian North // Proceedings of International Conference on Environmental Observations, Modeling and Information Systems ENVIROMIS-2010, 5 July – 11 July 2010, Tomsk: 43.

Kolmakova M.V, Kouraev A.V., Zakharova E.A., Kirpotin S.N., Zemtsov V.A., Mognard N.M. Hydrological and hydrochemical processes in the Western Siberian plain from remote and field observations // EGU Leonardo Topical Conference Series on the hydrological cycle. 10-12 November, 2010. Luxembourg.

Kolmakova M.V, Kouraev A.V., Zakharova E.A., Kirpotin S.N., Zemtsov V.A., Mognard N.M. Spatial and temporal variability of the hydrological regime and water quality in the cryolythozone of the

Western Siberia. //Proceedings of the conference "Fundamental problems of water and water resources, 24-28 Aug 2010, Barnaul, Russia

Kolmakova M.V, Kouraev A.V., Zakharova E.A., Kirpotin S.N., Zemtsov V.A., Mognard N.M. Natural regimes of the North-Western Siberian Wetlands: hydrological and ecological indicators // Enviromis-2010, 5-11 July, 2010, Tomsk, Russia.

Kouraev, A, Zakharova, EA, Samain, O, Mognarda NM, Cazenave A. Ob' river discharge from TOPEX/Poseidon satellite altimetry (1992–2002). Remote Sensing of Environment 93, 238– 245, 2004

Kouraev, AV, Kostianoy, AG, Lebedev, SA. Ice cover and sea level of the Aral Sea from satellite altimetry and radiometry (1992–2006). Journal of Marine Systems 76, 272–286, 2009

Kouraev A.V., A. Cazenave, N.M. Mognard, J-F Crétaux, S. Biancamaria, F. Rémy, B. Legrésy, P. Van Beek, E. Zakharova, I. G. Polikarpov, F. Al-Yamani, M.V. Kolmakova, Bazanov V.A., Skugarev A.A., Berezin A.E., Zemtsov V.A., Kirpotin S.N. From wet to arid zones: continental hydrology from satellite multi-sensor data and in situ observations. ESA living planet symposium, Bergen 2010.

Kouraev Alexei V., Michail N. Shimaraev, Frédérique Rémy, Andrei Yu. Ivanov, Boris N. Golubov An interesting natural phenomenon - giant rings on Lake Baikal ice. EGU-2010, Vienna

Kouraev Alexei V., Michail N. Shimaraev, Frédérique Rémy, Andrei Yu. Ivanov, Boris N. Golubov Giant rings on ice of the Lake Baikal: a look from space and from beneath. ESA living planet symposium, Bergen 2010.

Kouraev Alexei V., Michail N. Shimaraev, Frédérique Rémy, Andrei Yu. Ivanov, Boris N. Golubov Giant ice rings on Lake Baikal ice – potential causes, development and satellite monitoring. Workshop on Cold Regions Hydrology, Innsbruck, 2010

Kwok, R., G. F. Cunningham, M. Wensnahan, I. Rigor, H. J. Zwally, and D. Yi (2009), Thinning and volume loss of the Arctic Ocean sea ice cover: 2003–2008. J. Geophys. Res. 114, C07005, doi:10.1029/2009JC005312.

Kwok, R., Morison, J., Jan. 2011. Dynamic topography of the ice-covered arctic ocean from ICESat. Geophysical Research Letters 38 (2), L02501+.

Lawrence, D. M., A. G. Slater, R. A. Tomas, M. M. Holland and C. Deser (2008), Accelerated Arctic land warming and permafrost degradation during rapid sea ice loss, Geophys. Res. Lett., 35, L11506, doi:10.1029/2008GL33985.

Lemke, P. et al. (2007), Observations : changes in snow, ice and frozen ground. In: Climate change 2007: The physical Science Basis. Contribution of Working Group I to the Fourth Assessment report of the Intergovernmental Panel on Climate Change [Solomon S., D. Qin, M. Manning, Z. Chen, M. Marquis, K.B. Averyt, M. Tignor and H.L. Miller (eds.)]. Cambridge University Press, Cambridge, UK, and New York, USA.

Masarie, K. A. and P. P. Tans, 1995, Extension and integration of atmospheric carbon-dioxide dara into a globally consistent measurement record, J. Geophys. Res., 100(D6), 11593-11610.

Mognard, N. and E.G. Josberger, 2002, "Northern Great Plains 1996/97 seasonal evolution of snowpack parameters from satellite passive-microwave measurements", Annals of Glaciology,

MONARCH-A

**MONitoring and Assessing Regional Climate change in
High latitudes and the Arctic**
Grant agreement n° 242446

Ref: D4.2-y2
Date: 27/03/2012
Issue: 3

vol. 34, 15-23.

Neftel, A., H. Friedli, E. Moor, H. Lötscher, H. Oeschger, U. Siegenthaler, and B. Stauffer. 1994. Historical CO_2 record from the Siple Station ice core. In Trends: A Compendium of Data on Global Change. Carbon Dioxide Information Analysis Center, Oak Ridge National Laboratory, U.S. Department of Energy, Oak Ridge, Tenn., U.S.A. (http://cdiac.ornl.gov/trends/CO$_2$/siple.html).

Olsen, A., Key, R.M., Jeansson, E., Falck, E., Olafsson, J., Van Heuven, S., Skjelvan, I., Omar, A., Olsson, K.A., Anderson, L.A., Jutterström, S., Rey, F., Johannessen, T., Bellerby, R.G.J., Blindheim, J., Bullister, J.L., Pfeil, B., Lin, X., Kozyr, A., Schirnick, C., Tanhua, T., Wallace, D.W.R., 2009. Overview of the Nordic Seas CARINA data and salinity measurements. Earth Syst. Sci. Data 2, 1-25.

Omar, A.M., Johannessen, T., Kaltin, S., Olsen, A., 2003. Anthropogenic increase of oceanic pCO2 in the Barents Sea surface water. Journal of Geophysical Research 108 (C12)

Peters, G. P., G. Marland, C. Le Quéré, T. Boden, J. G. Canadell, and M. R. Raupach, 2012, Rapid growth in CO_2 emissions after the 2008–2009 global financial crisis, correspondence (opinion&comment), Nature Climate Change, 2, January 2012, 1-4.

Piaoa, S , P. Ciais , M. Lomas, C. Beer , H. Liu , J. Fang , P. Friedlingstein , Y. Huang , H. Muraoka , Y. Son , I. Woodward, Contribution of climate change and rising CO_2 to terrestrial carbon balance in East Asia: A multi-model analysis. Global and Planetary Change, doi: 10.1016/j.gloplacha.2010.10.014.

Pierrot, D., Neill, C., Sullivan, K., Castle, R., Wanninkhof, R., Luger, H., Johannessen, T., Olsen, A., Feely, R.A., Cosca, C.E., 2009. Recommendations for autonomous underway pCO(2) measuring systems and data-reduction routines. Deep-Sea Research Part Ii-Topical Studies in Oceanography 56 (8-10), 512-522.

Polyakov, I. V., A. Beszczynska, E. C. Carmack, I. A. Dmitrenko, E. Fahrbach, I. E. Frolov and R. Gerdes (2005), One more step toward a warmer Arctic. Geophys. Res. Lett. 32, 17. doi:10.1029/2005GL023740.

Proshutinsky, A., V. Pavlov, and R. H. Bourke, Sea level rise in the Arctic Ocean, Geophysical Research Letters, 28, 2237-2240, 2001.

Proshutinsky, A., I. M. Ashik, E. N. Dvorkin, S. Häkkinen, R. A. Krishfield, and W. R. Peltier (2004), Secular sea level change in the Russian sector of the Arctic Ocean. J. Geophys. Res., 109, C03042, doi:10.1029/2003JC002007.

Quegan S, Beer C, Shvidenko A, McCallum I, Handoh I C, Peylin P, Rödenbeck C, Lucht W, Nilsson S & Schmullius C (2011), Estimating the carbon balance of central Siberia using a geographical information system, atmospheric inversion and dynamic vegetation models, Global Change Biology, 17, 351–365.

Rignot, E., I. Velicogna, M. R. van den Broeke, A. Monaghan and J. Lenaerts (2011), Acceleration of the contribution of the Greenland and Antarctic ice sheets to sea level rise, Geophys. Res. Lett., 38, L05503

Rudels, B., Jones, E.P. and Anderson, L.G., 1994. On the intermediate depth waters of the Arctic Ocean. In: Johannessesn, O.M., Muench, R.D. and Overland, J.E., Editors, 1994. The polar

MONARCH-A

MONitoring and Assessing Regional Climate change in High latitudes and the Arctic
Grant agreement n° 242446

Ref: D4.2-y2
Date: 27/03/2012
Issue: 3

oceans and their role in shaping the global environment, The Nansen Centennial Volume, pp. 33–46.

Semtner, A. J.: A model for the thermodynamic growth of sea ice in numerical investigations of climate, J. Phys. Oceanogr., 6, 379–389, 1976.

Serra, N., Käse, R. H., Köhl, A., Stammer, D., Quadfasel, D., 2010. On the low-frequency phase relation between the denmark strait and the Faroe-Bank channel overflows. Tellus A 62 (4), 530-550.

Siegenthaler, U., T. F. Stocker, E. Monnin, D. Lüthi, J. Schwander, B. Stauffer, D. Raynaud, J.-M. Barnola, H. Fischer, V. Masson-Delmotte, and J. Jouzel, 2005, Stable Carbon Cycle–Climate Relationship During the Late Pleistocene, Science, 310, 1313- 1317.

Smith, L. C., Y. Sheng, G. M. MacDonald, and L. D. Hinzman (2005), Disappearing arctic lakes. Science, 308, 1429.

Spreen, G., S. Kern, D. Stammer, and E. Hansen (2009), "Fram Strait sea ice volume export estimated between 2003 and 2008 from satellite data", Geophys. Res. Lett., 36, L19502, doi:10.1029/2009GL039591.

Steele, M., R. Morley, and W. Ermold, PHC: A global ocean hydrography with a high quality Arctic Ocean, J. Climate, 14, 2079-2087, 2001.

Stroeve, J., M. M. Holland, W. Meier, T. Scambos and M. Serreze (2007), Arctic sea ice decline: faster than forecast, Geoph. Res. Lett., 34, L09502, doi:10.10292007GL029703.

Sørensen, LS, S. B. Simonsen, K. Nielsen, P. Lucas-Picher, G. Spada, G. Adalgeirsdottir, R. Forsberg, C. S. Hvidberg: Mass balance of the Greenland ice sheet (2003–2008) from ICESat data – the impact of interpolation, sampling and firn density, The Cryosphere, 5, 173-186, 2011, doi:10.5194/tc-5-173-2011, www.the-cryosphere.net/5/173/2011

Sørensen, LS, L. Stenseng, S. B. Simonsen, R. Forsberg, S. K. Poulsen, V. Helm: Greenland Ice Sheet changes from space using laser, radar and gravity, ESA Living Planet Conference, ESA Special Publication SP-686, 2010.

Sørensen, L. S. , R. Forsberg, S. B. Simonsen, V. R. Barletta, H. Skourup: Changes of the Greenland Ice Sheet from ICESat, CryoSat and GRACE. Oral presentation at American Geophysical Union (AGU) fall meeting, San Francisco, California, USA. December 5-9, 2011

Sørensen, L. S.: Monarch-A D2.3.2 Grid of ICESat height changes, average trend 2003-2008, September 2011

Tanhua, T., Steinfeldt, R., Key, R.M., Brown, P., Gruber, N., Wanninkhof, R., Perez, F., Körtzinger, A., Velo, A., Schuster, U., Van Heuven, S., Bullister, J.L., Stendardo, I., Hoppema, M., Olsen, A., Kozyr, A., Pierrot, D., Schirnick, C., Wallace, D.W.R., 2009a. Atlantic Ocean CARINA data: overview and salinity adjustments. Earth Syst. Sci. Data 2, 241-280.

Tanhua, T., Van Heuven, S., Key, R.M., Velo, A., Olsen, A., Schirnick, C., 2009b. Quality control procedures and methods of the CARINA database. Earth Syst. Sci. Data 2, 205-240.

Tjiputra, J.F., K. Assmann, M. Bentsen, I. Bethke, O.H. Otterå, C. Sturm, and C. Heinze, 2010a, Bergen earth system model (BCM-C): Model description and regional climate-carbon cycle feedbacks assessment, Geoscientific Model Development, 3, 123–141

Tjiputra, J.F., K. Assmann, and C. Heinze, 2010b, Anthropogenic carbon dynamics in the changing ocean, Ocean Science, 6, 605–614

Wania R., Ross I., and Prentice I.C., 2009, Integrating peatlands and permafrost into a dynamic global vegetation model: 1.Evaluation and sensitivity of physical land surface processes, Global Biochem. Cycles , 23, GB3014.

Woodward, .F. I., Lomas M. R., 2004, Vegetation dynamics – simulating responses to climatic change, Biol. Rev., 79, pp. 643–670.

Zakharova E.A., A.V. Kouraev, S. Biancamaria, M.V. Kolmakova, N.M. Mognard, V.A. Zemtsov, S.N. Kirpotin, B. Decharme. Snow cover and spring flood flow in the northern part of the Western Siberia (the Poluy, Nadym, Pur and Taz rivers). Journal of Hydrometeorology, 2011 (submitted)

Zakharova E.A., Kouraev A.V., Kolmakova M.V., Bazanov V.A., Skugarev A.A., Berezin A.E., Kirpotin S.N., Zemtsov V.A., Biancamaria S., Mognard N.M. Seasonal and interannual changes of hydrological regime of the Western Siberia. EGU-2010, Vienna

Zakharova E.A., Kouraev A.V., Kolmakova M.V., Bazanov V.A., Skugarev A.A., Berezin A.E., Kirpotin S.N., Zemtsov V.A. Mognard N.M. Hydrology of the Western Siberia - seasonal and interannual changes. ESA living planet symposium, Bergen 2010.

Zakharova E.A., Kouraev A.V., Biancamaria S., Kolmakova M.V., Kirpotin S.N., Zemtsov V.A. Mognard N.M. Role of wetlands in the seasonal distribution of discharge of the Poluy, Nadym, Pur and Taz rivers. Workshop on Cold Regions Hydrology, Innsbruck, 2010

END OF DOCUMENT